The Modeled Response of the Mean Winter Circulation to Zonally Averaged SST Trends

GUDRUN MAGNUSDOTTIR

Department of Earth System Science, University of California, Irvine, Irvine, California

(Manuscript received 27 July 2000, in final form 23 May 2001)

ABSTRACT

The response of the atmospheric winter circulation in both hemispheres to changes in the meridional gradient of sea surface temperature (SST) is examined in an atmospheric general circulation model. Climatological SSTs are employed for the control run. The other runs differ in that a zonally symmetric component is added to or subtracted from the climatological SST field. The meridional structure of the variation in SST gradient is based on the observed change in zonally averaged SST over the last century. The SST trend has maxima of about 1 K at high latitudes of both hemispheres. Elsewhere, the increase in SST over the last century is fairly uniform at about 0.5 K.

In both hemispheres the response to decreased SST gradients is decreased baroclinity in the lower troposphere and increased baroclinity in the upper troposphere, with the reverse response when the SST gradient is increased. Because the cases with decreased SST gradients correspond to warmer SSTs everywhere, they are accompanied by an increase in moisture and a general expansion of the troposphere. The warming cases in the Northern Hemisphere (NH) winter are marked by greatly increased tropical convection, a stronger subtropical jet that is shifted upward and equatorward, and a robust stationary-wave response. Many aspects of the response are remarkably consistent among the different warming experiments, both in pattern and amplitude. The storm-track response is weaker but still consistent among the different warming experiments. Despite general decrease in storm-track activity, there is a tendency for the upper-level NH storm tracks to strengthen at their downstream end and to weaken at their upstream and northward end. When the zonally symmetric SST anomaly field is subtracted from the climatological SST (resulting in lower SST with increased latitudinal gradient), the response is different in many fields and is considerably weaker.

In the winter Southern Hemisphere the change in baroclinity of the low-level flow plays a greater role in the response than in the winter NH. The response in the storm track is zonal with a decrease in midlatitude storm-track activity in the warming cases and an increase in the case that has an increased SST gradient (and cooler SST). There is close correspondence between the pattern of response in all the experiments, irrespective of the sign of the SST anomaly field.

1. Introduction

It remains a high priority to understand the sensitivity of the atmospheric circulation to changes in boundary forcing, especially to variations in sea surface temperature (SST) and sea-ice distribution. To date, the effects of varying boundary forcing have been studied less than the effects of varying composition even though an increase in greenhouse gas concentrations has been strongly linked to an increase in surface temperature. In this study we address the effects of zonally symmetric trends in SST, corresponding to centennial and longer timescales, on the winter-mean circulation in each hemisphere.

The effects of extratropical SST anomalies on the atmospheric circulation are less well understood than the effects of tropical SST anomalies, largely because of the much larger internal variability of the midlatitude atmosphere, which tends to obscure any direct effect of the SST anomaly. Robinson (2000) has recently summarized the current state of knowledge as regards observational and modeling studies of the atmospheric response to isolated midlatitude SST anomalies. The response of atmospheric general circulation models (GCMs) to interannual SST anomalies is weak, but not negligible, and is quite nonlinear to the amplitude and sign of change. The response is also nonlinear in terms of geographical regions, such that the effects of SST anomalies in different regions are not additive. Several modeling studies have found that the response is highly sensitive to the location of the SST anomaly relative to the storm track and the mean jet as well as to the jet strength. This latter result is rather worrisome in light of the fact that some of the models have significant errors in the location and strength of these features.

Corresponding author address: Dr. Gudrun Magnusdottir, Department of Earth System Science, University of California, Irvine, Irvine, CA 92697-3100.
E-mail: gudrun@uci.edu

Here the focus is on examining the response to SST change corresponding to longer timescales than many previous studies. The expectation is that the atmosphere will respond robustly to changes in SST corresponding to an entirely different oceanic heat transport. Natural and anthropogenic climate variations could both lead to changes in the meridional heat transport in the ocean, which would be reflected in changes in the SST distribution. Rather than trying to distinguish between these two different effects, we simply use the observed changes in SST over the past century to define a characteristic latitudinal profile of SST variability. Different amplitudes of this zonally uniform characteristic SST variability pattern are added to (or subtracted from) the climatological SST distribution to generate different scenarios of global SST variability. Each of these SST scenarios will, of course, correspond to a different implied oceanic heat transport. Five such SST scenarios are used as surface boundary conditions to force an atmospheric GCM.

This is a follow-up study to Magnusdottir and Saravanan (1999, hereinafter MS99) in that the same GCM experiments are analyzed, but here the emphasis is on the dynamical response of the winter-mean circulation in each hemisphere. The primary focus of MS99 was to examine the response of the vertical boundary fluxes of energy, as well as the response of the vertically integrated, atmospheric meridional heat transport and its various decompositions to a change in the implied oceanic heat transport. They found that in the annual mean, the atmosphere adjusts such that the total meridional heat transport (by atmosphere and ocean) is not sensitive to the change in zonally averaged SST, which is consistent with the results of Rind (1998). MS99 also noted a large degree of compensation even between the different components of atmospheric heat transport such that changes in latent heat transport usually go hand in hand with changes in dry static energy transport of an opposite sign. As MS99 discussed, given great resources our simulations would have been carried out using a sophisticated, coupled climate model, which is very expensive to run. Since we had limited resources and our primary interest was in the atmospheric response to different scenarios of oceanic heat transport, we took the frugal approach of forcing a realistic atmospheric GCM with the different SST distributions, irrespective of how the ocean might have come to the state of having the different SST distributions.

The annual-mean, zonally averaged centennial SST trend has maxima of about 1 K at high latitudes of both hemispheres. Elsewhere, the change in SST over the last century is fairly uniform at about 0.5 K. Since the SST is changed the most at high latitudes, resulting in a change in the meridional SST gradient and thus baroclinity, it is natural to focus on the response of the stationary waves and storm tracks. MS99 found that the winter-mean Northern Hemisphere (NH) heat transport due to transient eddies was sensitive to the change in SST gradient, consistent with a change in baroclinity. The stationary waves depend on zonal inhomogenities. Therefore it is not surprising that the winter heat transport due to stationary eddies was sensitive to the change in SST. Only vertically and longitudinally integrated quantities were considered in MS99. We attributed the high level of compensation between changes in ocean heat transport and variability in atmospheric heat transport at least in part to the high dynamical efficiency of atmospheric eddy transport. Here, we want to examine the response of the winter storm tracks and stationary eddies in more detail. We shall examine the dynamical response in the upper troposphere and the transient heat and moisture fluxes in the lower troposphere. Also, we want to determine whether (for any of the fields) there is some correspondence between the different experiments in terms of the amplitude of the zonally uniform SST change.

MS99 found that the two experiments corresponding to the largest increase in SST showed an increase in annual-mean, globally averaged, surface temperature that is similar to the values obtained in scenarios for global warming. Moreover, the surface temperature increase over land in these two experiments was greater than the globally averaged value. Of course, the atmospheric composition was not explicitly changed and oceanic properties such as SSTs were prescribed. Note that some greenhouse gas changes affect the vertical structure of the atmosphere, which was not considered in these experiments. Another very important effect of changing the atmospheric composition is to increase the land surface temperatures directly through radiation. In the warming experiments, the increase in land surface temperature took place only because of the SST change and the associated changes in atmospheric moisture. Even without explicitly changing the atmospheric conditions over land, the average temperature increase over land was greater than the globally averaged temperature increase. This implies that the direct effects of changing atmospheric composition and thereby changing the radiation may be far less important than the indirect effects of a changed moisture content. Here we shall further compare the winter-mean response in our experiments to results from global change scenarios. Some striking similarities appear. Since the atmosphere is forced by surface heating this is not as far fetched as it might seem at first. Note, however, that both natural and anthropogenic climate variations give rise to the latitudinal structure of the SST anomaly that is used to force the current simulations. Also, the SST anomaly is that corresponding to the centennial trend and multiples thereof. These timescales are longer than global change scenarios typically consider. An area of much current interest is how regional climate features such as the winter storm tracks might be displaced or changed in a global change scenario. Several studies have considered the response of the NH storm tracks to increased concentration of carbon dioxide. Most find that the NH storm tracks are

amplified at the downstream end (e.g., Carnell et al. 1996; Schubert et al. 1998; Ulbrich and Christoph 1999). Others find also a northward shift in the North Atlantic storm track (e.g., Hall et al. 1994). Fewer studies have considered the effects of climate forcing on the Southern Hemispheric (SH) storm track, which is surprising in light of the simpler land–sea configuration in that hemisphere that should help in interpreting results. In this paper, I am particularly interested in the extratropical response to the SST forcing although strong tropical response will be noted.

The plan of the paper is as follows: Section 2 gives an overview of the model, the numerical experiments, and data analysis used, as well as a summary of the model's performance in simulating the atmospheric circulation with climatological SSTs. Section 3 contains results for the December–February (DJF) mean response in the NH. Section 4 contains results for the winter season [June–August (JJA)] of the SH. Section 5 contains some concluding remarks.

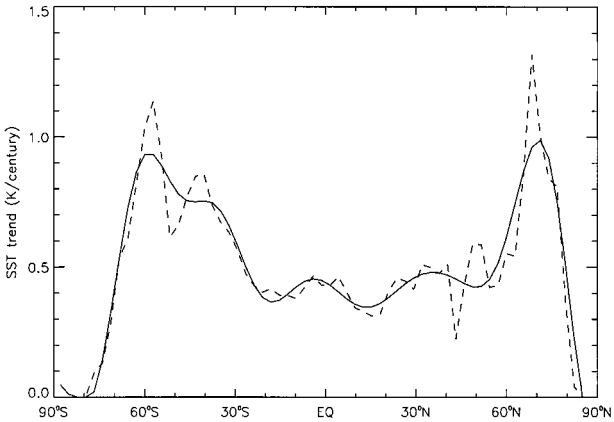

FIG. 1. Least squares trend in annual-mean, zonally averaged SST (K century^{-1}) from GISST2 data as a function of latitude. The dashed curve represents the raw data. The solid curve represents the data after spatial smoothing.

2. Some preliminaries

a. Model, experiments, and the global response

The numerical model is the National Center for Atmosphere Research (NCAR) Community Climate Model, version 3 (CCM3), in the standard configuration as detailed in Kiehl et al. (1998). The model resolution is T42 with 18 vertical layers in a hybrid-sigma coordinate system. This version of CCM presents major improvements over earlier versions especially in terms of the physical parameterizations resulting in a more realistic thermal structure and hydrologic cycle. Hack et al. (1998) present a comprehensive study of the simulated hydrologic and thermodynamic characteristics of CCM3 based on a 15-yr integration using observed monthly mean SSTs from 1979 to 1993. Hurrell et al. (1998) use the same 15-yr simulation to examine the dynamical representation of CCM3. This simulation is almost identical to the control case, 0X, which is a 10-yr simulation using 1 yr of climatological monthly mean SSTs that are repeated each year. The prescribed boundary forcing is determined from monthly mean SST fields, linearly interpolated in time between months. Sea ice is prescribed in the model whenever the SST goes below the threshold value of -1.8°C. MS99 discussed the problems associated with the melting of considerable amounts of sea ice when the SST is raised only slightly. Since sea ice is not explicitly represented in the model, only surface properties such as albedo and the surface energy fluxes change when the sea surface is covered by ice.

Figure 1 shows the spatial structure of the SST perturbation that is added to the SST for each month of the year. This structure is based on the annual-mean, zonally averaged least squares trend in the Global Sea Ice and SST (GISST2) dataset (Rayner et al. 1995), which extends from 1903 to 1994. As displayed in the figure, the trend is scaled to correspond to the centennial trend in SST and has maxima at high latitudes (poleward of 60° latitude) in both hemispheres of about 1 K, and is fairly constant at 0.5 K at other latitudes. The different experiments vary in terms of the amplitude of the perturbation, not its meridional structure. The term ''trend factor'' is used to refer to the factor by which the centennial trend in zonally averaged SSTs is multiplied in each experiment before adding it to the SST field. In what follows, I shall discuss five different cases, characterized by trend factors 0X, 1X, 5X, -5X, and 9X, respectively: 1) a control simulation, using climatological SST, denoted by 0X or control; 2) a simulation, denoted by 1X, that has SST such that the centennial trend is added to the climatological SST; 3) a simulation, denoted by 5X, that has SST such that 5 times the centennial trend is added to the climatological SST; 4) a simulation, denoted by -5X, that has 5 times the centennial trend subtracted from climatological SST; and 5) a simulation, denoted by 9X, that has 9 times the trend added to the climatological SST.

Choosing this particular meridional structure to the SST perturbation (based on observations) provides for a certain degree of realism. The fact that the perturbation is applied over all the oceans distinguishes this study from the typical extratropical *isolated* SST anomaly studies that were reviewed by Robinson (2000) and the effects of which were found to be rather weak. When we examined the latitude–longitude structure of the SST trend (before taking the zonal average of SST), it was very noisy. The trend in zonally averaged SST, before spatial smoothing (shown by the dashed curve in Fig. 1), is still noisy, but a very distinct meridional signature is apparent. As we shall see, even the zonally averaged and spatially smoothed SST anomaly pattern provides for an interesting response that in some fields is similar to the response in global change scenarios. Additionally,

TABLE 1. (a) The different numerical experiments and the associated trend factor (first column) indicating the DJF-mean change in globally averaged surface temperature (second column, K) from the control (0X). The third column shows the resulting change in globally averaged rainfall rate (mm season^{-1}). (b) Same as (a) but for JJA means.

(a) DJF

Experiment (trend factor)	$\Delta T_{\text{sfc,}}$ K (global)	Δrainfall, mm season^{-1} (global average)
1X	1.6	4.6
5X	3.8	23.3
9X	6.0	41.8
−5X	−2.9	−21.1
Experiment (trend factor)	$T_{\text{sfc,}}$ K (global)	Rainfall, mm season^{-1} (global average)
0X	285.8	273.0

(b) JJA

Experiment (trend factor)	$\Delta T_{\text{sfc,}}$ K (global)	Δrainfall, mm season^{-1} (global average)
1X	1.4	3.8
5X	3.6	19.9
9X	5.8	35.7
−5X	−3.4	−20.0
Experiment (trend factor)	$T_{\text{sfc,}}$ K (global)	Rainfall, mm season^{-1} (global average)
0X	288.7	284.2

the fact that the spatial structure of the SST perturbation only depends on latitude, highlights the effect of the lower-tropospheric reduced baroclinity in the warming experiments (where a multiple of the perturbation is added to the climatological SST) on the resulting circulation. This is the so-called ''polar amplification'' effect. However, as we shall see, the global SST is simultaneously increased, resulting in a more robust hydrologic cycle. Conversely, the −5X experiment corresponds to increased baroclinity in the lower troposphere, lower SSTs, and a less active hydrologic cycle. This is reflected in the change in seasonal mean rainfall rate in Table 1.

At first glance the different experiments seem to correspond to vast changes, but as was emphasized by MS99, the resulting annual-mean, globally averaged, surface temperature change stays within the values usually found in double carbon dioxide scenarios. Table 1a shows the DJF-mean response in globally averaged surface temperature as well as rainfall rate for each of the experiments. Table 1b shows the same fields for the JJA mean. An increase in globally averaged DJF-mean and JJA-mean temperature goes hand in hand with an increase in precipitation rate. A decrease in globally averaged DJF-mean and JJA-mean temperature in the −5X experiment is accompanied by a decrease in precipitation rate. Comparing the two tables, note that the response in the 5X and −5X cases tend to be more symmetrical in JJA than in DJF, both in terms of temperature and rainfall. In MS99 (their Fig. 8), we showed the various components of the zonally averaged, annual-mean surface heat flux response. We have also examined the seasonal-mean net surface flux response. The response is negative almost everywhere in the warming experiments (the response in net flux is directed into the atmosphere), and positive in the −5X case.

In this paper I chose to mainly show results for the two cases, 5X and −5X. The response in the time-mean fields of these two cases (as well as for the more strongly forced 9X case) is statistically significant almost everywhere at the 95% level, using a *t* test. Even though the 1X response is weaker and therefore not as statistically significant, it is consistent with the 5X and 9X response, which is reassuring. The *t* test is not appropriate for testing statistical significance of the response in the variance and covariance fields, and each time series is too short for reliable significance results by other tests. However, the fact that there is close correspondence between the corresponding fields for the different experiments lends credibility to their statistical significance.

b. Data analysis and diagnostics

In MS99 we examined the winter-mean atmospheric heat transport for each of the experiments. We divided the heat transport in each case into an eddy contribution and a mean meridional contribution. The eddy heat transport was further divided into a contribution due to stationary eddies and a contribution due to transient eddies. Both showed pronounced response, the heat transport due to stationary eddies in the NH winter and that due to the transient eddies in both winter hemispheres. Here, I shall examine the response in more detail. It is well known that the transient eddies are particularly spatially localized if the high-frequency part is separated from the low-frequency part, which is generally taken to be of longer timescale than 6–10 days. To represent the high-frequency eddies that characterize the winter storm tracks, I processed the data using a bandpass filter that retains fluctuations with 2–8-day periods. I chose to examine winter means by averaging over each of the three solsticial months, DJF and JJA. Each of the experiments was almost 10 yr long with the instantaneous dynamical fields saved 2 times per day. (For DJF we have results for all 10 yr or 30 months, for JJA we have results for 27 months.) In what follows, I use square brackets to represent a zonal average and the star to represent the deviation from the zonal average (e.g., $x = [x] + x^*$). The overbar represents a time mean over the three months (DJF or JJA) of all 10 yr of simulation, and the prime represents the deviation from the time mean (e.g., $x = \overline{x} + x'$). When I examine time-mean fields that are quadratic in transient eddy variables (e.g., $\overline{x'y'}$), it is implicit that the fields are time filtered

so that only variations of 2–8-day timescale are included.

I chose to characterize the upper-level response of the flow primarily by the streamfunction field, denoted by $\overline{\psi}$. The stationary waves are depicted in terms of $\overline{\psi^*}$, the deviation of the mean streamfunction from zonal symmetry. The upper-level storm tracks are depicted by the time-filtered variance field of the 250-hPa streamfunction, denoted by $\overline{\psi'^2}$. The structure of the storm tracks as shown by this field is very similar to the time-filtered eddy kinetic energy. Barotropic effects, such as the transient eddy vorticity flux, are particularly important toward the rear of the storm track, at tropopause level. By contrast, baroclinic effects, such as the transient eddy heat flux, are most important in the front area of the storm track, around the 700-hPa level. This is consistent with the view of the storm track as representing a collection of life cycles of baroclinic waves, each at a different stage in the life cycle, such that incipient systems are in the entrance region with decaying systems toward the end. It is well established (e.g., Edmon et al. 1980) that during the growth of such a baroclinic disturbance, the lower-level transient heat flux is most important early on, making way to the transient momentum flux at upper levels during the mature and decaying phases of development.

One can use simple barotropic arguments to attempt to infer how the transients are influencing the upper-level mean flow. At the level of quasigeostrophic theory, the inviscid, time-mean vorticity equation may be written as

$$\left(\frac{\partial}{\partial t} + \overline{\mathbf{v}} \cdot \boldsymbol{\nabla}\right)\overline{\zeta} + f\overline{D} + \boldsymbol{\nabla} \cdot \overline{\mathbf{v}'\zeta'} = 0,$$

where ζ is absolute vorticity, $\mathbf{v} = (-\psi_y, \psi_x)$ is the horizontal geostrophic flow, D is divergence, and f is the planetary vorticity. One can rewrite this equation in terms of streamfunction as follows:

$$\left(\frac{\partial}{\partial t} + \overline{\mathbf{v}} \cdot \boldsymbol{\nabla}\right)\overline{\psi} = -\nabla^{-2}(\boldsymbol{\nabla} \cdot \overline{\mathbf{v}'\zeta'}) - \nabla^{-2}(f\overline{D}).$$

The first term on the rhs is the barotropic forcing of the mean streamfunction by the high-frequency transients. The transient eddy vorticity flux has a maximum near the tropopause, so that this term, often referred to as $\overline{S}$ (Hoskins et al. 1983), is particularly important at upper levels, such as the 250-hPa level.

Baroclinic influences are most important around the 700-hPa level where the high-pass transient eddy heat flux is largest. It is of interest to examine the heat flux field at that level. Last, moisture affects the storm tracks greatly through latent heat release where the moisture condenses. The current experiments, where the change in SST is positive, resulting in global and local warming, amplify this effect because of the nonlinear dependence of saturation vapor pressure on temperature. Moisture falls off quickly with height. Thus the maximum in the transient moisture flux is lower than that of the heat flux, or around the 850-hPa level.

c. Comments on the simulated winter (DJF) circulation

An advantage of using CCM3 is that in addition to being well documented, many of the fields produced by climatological conditions in the model have been compared with the same fields as calculated from the National Centers for Environmental Prediction (NCEP) global reanalysis (Kalnay et al. 1996) for the same time period. In particular, Hack et al. (1998) present an overview of the hydrologic and thermodynamic characteristics of the model and Hurrell et al. (1998) present an overview of its dynamical characteristics. In general, the zonally averaged fields, time averaged over a season, show a close correspondence to the NCEP reanalysis fields. The upper-tropospheric, seasonal-mean dynamical fields similarly show a close correspondence with reanalysis data. This applies especially to the 250-hPa stationary wave field, as depicted by $\overline{\psi^*}$, where ψ is the streamfunction. This field for the DJF mean of the control simulation, 0X, is shown in Fig. 2b. The DJF-mean zonal wind at 250 hPa, shown in Fig. 2a, depicts the location of the two winter jets accurately on the west side of each NH ocean basin. As compared with NCEP data the Pacific jet is underrepresented in the model, but by less than 5 m s^{-1}, and the North Atlantic jet is too strong by about 5 m s^{-1}.

Fewer studies have examined the high-frequency, transient eddy variance and covariance fields in the model, as compared with reanalysis fields. The storm tracks are frequently characterized by the high-pass, time-filtered variance of the streamfunction or $\overline{\psi'^2}$, on an upper-tropospheric level. This field depicts the storm tracks in the 250-hPa DJF mean for 0X in Fig. 2c, as a belt of maximum $\overline{\psi'^2}$, extending from the Pacific across North America and the Atlantic into Europe. For confidence in the model's ability to simulate the midlatitude storm tracks, it is useful to compare the control simulation's depiction of this field for DJF to the same field as calculated from NCEP reanalysis data. I shall also pay particular attention to the model's representation of the upper-tropospheric transient eddy vorticity flux since it is less constrained in the climate system than the lower-tropospheric heat flux (e.g., Held and Phillips 1993). Here, I shall concentrate on the field $\overline{S}$, where $\overline{S} = -\nabla^{-2}(\boldsymbol{\nabla} \cdot \overline{\mathbf{v}'\zeta'})$ (see the previous section), on the 250-hPa surface. This field represents the barotropic forcing of the 250-hPa mean streamfunction by the high-frequency transient eddies. At the level of quasigeostrophic theory, the Laplacian of this term is the only conservative forcing of the mean vorticity at the 250-hPa level, aside from the term proportional to the mean divergence. Thus in addition to giving a smoothed representation of the 250-hPa transient eddy vorticity

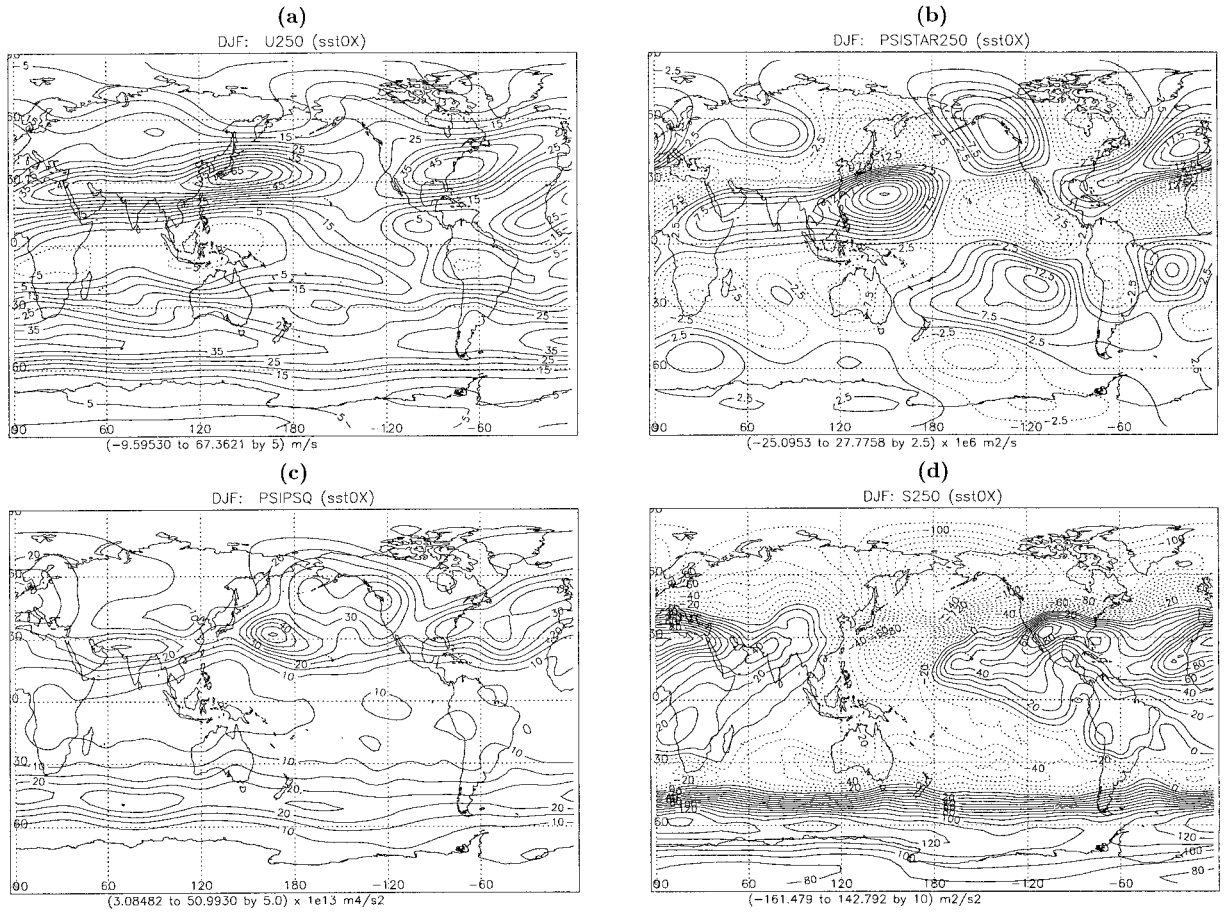

FIG. 2. DJF-mean fields for the control case (0X) on the 250-hPa surface. Negative contours are dashed. (a) Zonal wind (m s^{-1}), contour interval is 5. (b) Eddy streamfunction ($\overline{\psi^*}$, 10^6 m^2 s^{-1}), contour interval is 2.5. (c) High-frequency filtered transient eddy streamfunction variance (10^{13} m^4 s^{-2}), contour interval is 5. (d) Barotropic forcing of the mean streamfunction by the high-frequency filtered transient eddies (m^2 s^{-2}), contour interval is 10.

flux, it is also indicative of the eddy forcing of the mean rotational flow.

Two unrelated issues are unresolved. First, what are the systematic model errors in these two transient eddy fields (shown in Figs. 2c,d)? Second, it is unknown what type of sampling error to expect when considering only 30-month averages, in light of the considerable internal variability of the extratropical troposphere. I attempt to address these issues by examining the DJF-mean fields of $\overline{\psi'^2}$ and $\overline{S}$ computed from reanalysis data and comparing them with Figs. 2c,d.

Figure 3a shows the DJF averaged $\overline{\psi'^2}$ for 18 yr of NCEP reanalysis data (1979–97) that have the same spatial resolution as the model and a temporal resolution corresponding to 4 times per day. Figure 3b shows the same field for an 80-yr simulation of CCM3 applying climatological SST. We see that CCM3 (Fig. 3b) tends to underestimate the high-frequency transient variance especially in the North Atlantic. In the North Pacific there is a double maximum in this quantity. One is located in the exit region of the jet over the western part of the basin; the other is located farther poleward and at the North American coastline. The NCEP data only have one extensive maximum over the Pacific, stretching from the exit region of the jet to the WNW, reaching the North American coast. In the Atlantic, the CCM3 maximum in streamfunction variance stretches from the U.S. east coast, northward and eastward over Ireland and Wales. As compared with NCEP data, the maximum variance is too zonally elongated and the values are too low. Underestimating the high-frequency streamfunction variance is a common problem in GCMs. Comparing Fig. 3b to Fig. 2c, which shows the variance field for 0X, we see that the rather short time sample of only 10 yr (or 30 winter months), produces a North Atlantic storm track that is a bit further reduced in amplitude. Still, both the shape and location of the storm tracks are essentially the same for the shorter time series.

The field $\overline{S}$ depicts the barotropic forcing of the mean rotational flow by the transient eddies. The most pronounced feature in Fig. 2d, which depicts the 0X case, is the anticyclonic forcing stretching from the eastern

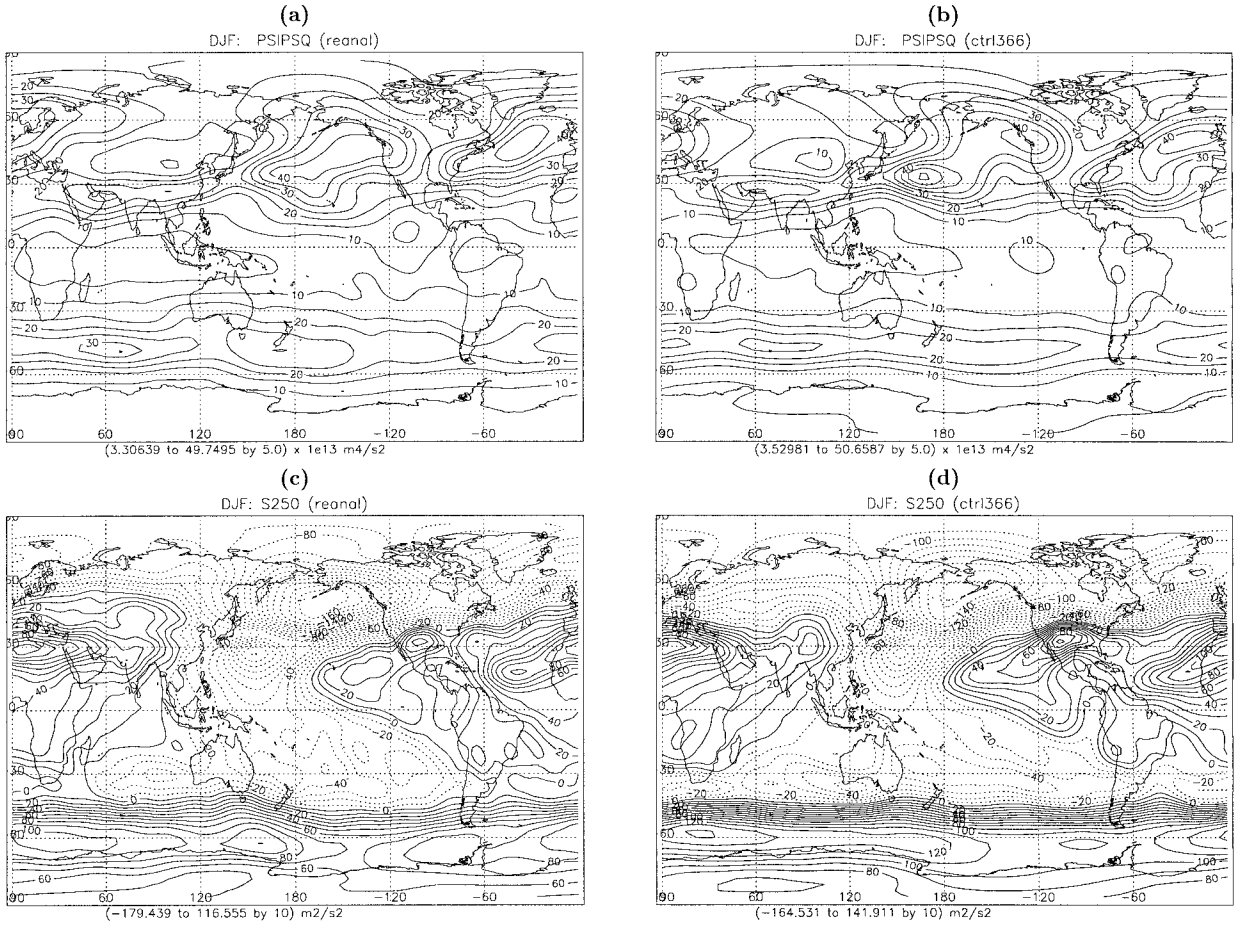

FIG. 3. DJF-mean fields at 250 hPa. Negative contours are dashed. (a) High-frequency filtered transient eddy streamfunction variance (10^{13} m^4 s^{-2}), for 18 yr of NCEP data. Contour interval is 5. (b) Same as (a) but for 80 yr of CCM3 control simulation. (c) Barotropic forcing of the mean streamfunction by the transient eddies (m^2 s^{-2}), for 18 yr of NCEP data. Contour interval is 10. (d) Same as (c) but for 80 yr of CCM3 control simulation.

Pacific east across the Atlantic into Eurasia. This leads to westerly acceleration, especially along the Atlantic storm track. This field is almost indistinguishable from the same field computed from the 80-yr simulation and shown in Fig. 3d. Thus sampling error does not seem to play a major role in this quite smoothed field of the 250-hPa transient eddy vorticity flux. The same field now calculated from NCEP data is shown in Fig. 3c. When compared with Fig. 3d, the general pattern is quite close, but the amplitude is considerably weaker in the reanalysis data. This is consistent with the fact noted earlier that the Atlantic westerly jet tends to be overestimated in the model. Other differences are also evident on closer inspection, such as the fact that the anticyclonic forcing over the Atlantic as depicted in the reanalysis data in Fig. 3c tends to be at more of a meridional angle than the corresponding model fields in Figs. 2d and 3d, which is consistent with the more zonal orientation of the Atlantic storm track and jet in CCM3 as compared with NCEP reanalysis.

I conclude that even though there is systematic error in the depiction of the midlatitude storm tracks, this error is less pronounced than in many other GCMs (e.g., Kageyama et al. 1999). Additionally, the sampling error is minor.

3. The DJF-mean NH response

a. Main features of the response

The DJF-mean, zonally averaged, NH response is quite linear in the sign and magnitude of the trend factor of SST change, aside from the low-level, high-latitude thermodynamic response, some of which is artificial and associated with the change in sea ice. The response is shown for 5X in Fig. 4. The structure of the response in temperature when SST is warmed is very similar to GCM experiments with doubled CO_2 concentration (e.g., Hall et al. 1994). This signal consists of the strongest warming in the free troposphere taking place in the tropical upper troposphere so that the meridional temperature gradient is increased at upper levels while it is

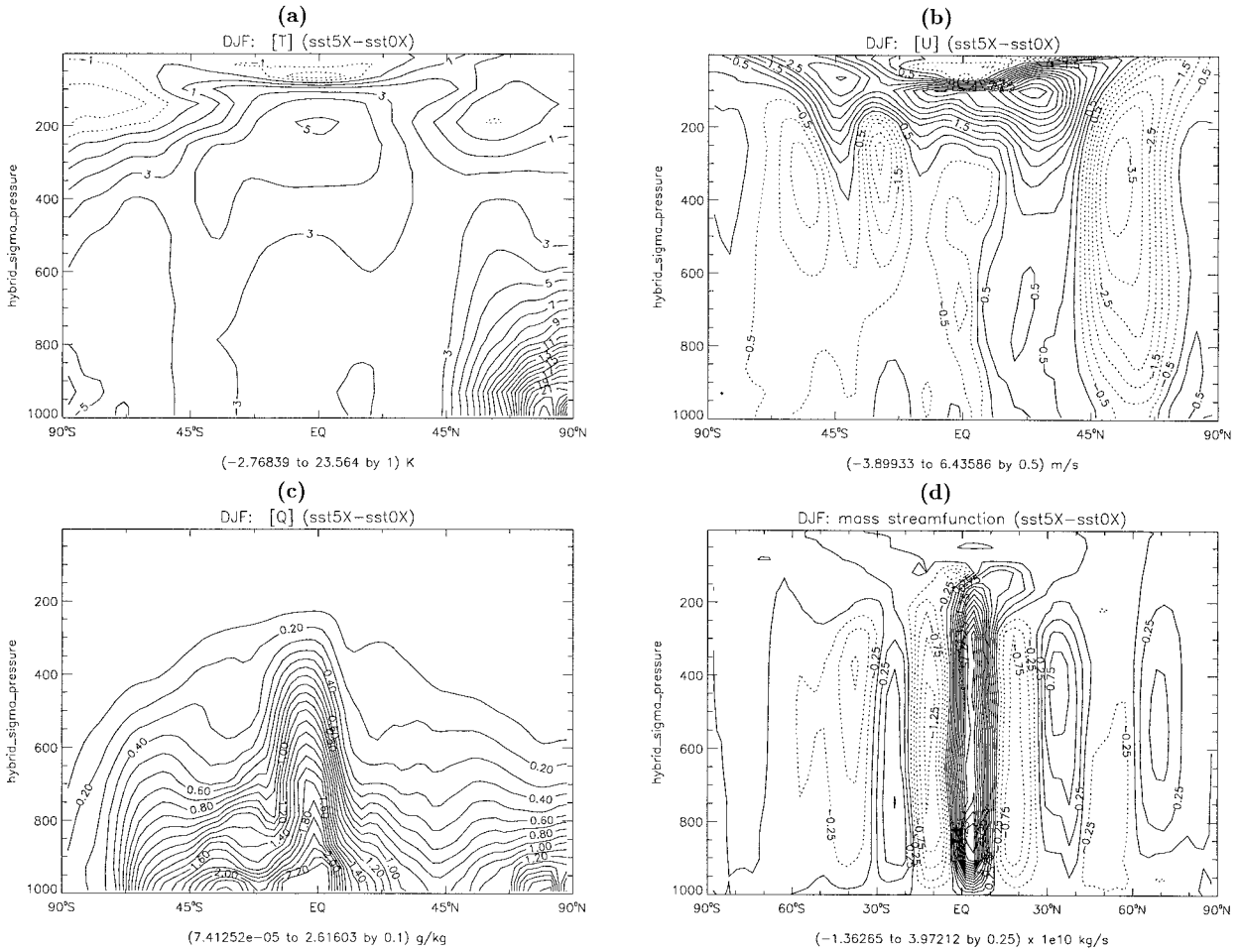

FIG. 4. DJF-mean, zonally averaged response (deviations from 0X) for the 5X case. Negative contours are dashed. (a) Temperature response. Contour interval is 1 K. (b) Zonal wind response in meters per second. Contour interval is 0.5. (c) Specific humidity response in grams per kilogram. Contour interval is 0.1. (d) Mass streamfunction in 10^{10} kilograms per second. Contour interval is 0.25.

decreased at low levels. This signature is a result of the fact that at warmer surface temperatures, a low-latitude air parcel has a higher saturation vapor pressure and can thus release more heat as that moisture condenses in a rising air parcel. The exact magnitude of this effect is sensitive to the parameterization of convection in the model. The −5X experiment (not shown), where SST is cooled the most at high latitudes, shows a reversed signal of decreased upper-level temperature gradient and cooling throughout the troposphere with warming in the stratosphere.

The response in the zonally averaged zonal wind is such that the upper-level westerlies strengthen substantially and the tropical easterlies all but disappear for the 5X and 9X cases where the meridional temperature gradient has increased in the upper troposphere. This leads to an upward and equatorward displacement of the subtropical jet. Zonal wind for these cases is decreased through a deep layer at mid- to high latitudes of the NH. In the lower troposphere these are areas where the meridional temperature gradient has been decreased, consistent with thermal wind balance. Only the 5X response is shown in Fig. 4b, but there is a close correspondence between the spatial distribution (outside of the SH) of change in zonal-average zonal wind for 5X and the opposite change for −5X. In the NH extratropics, the amplitude of this response is smaller for −5X, corresponding to the smaller surface temperature response at high latitudes.

The 5X response in specific humidity in Fig. 4c shows a close correspondence to the change in surface temperature, and the vertical extent in the equatorial region is strongly tied to the change in the Hadley circulation as depicted for 5X in Fig. 4d. The winter Hadley circulation is the most pronounced feature in the DJF-mean mass streamfunction (e.g., Peixoto and Oort 1992), showing a direct circulation (positive mass streamfunction) from low latitudes south of the equator to 30°N. Both 5X and 9X show a substantial increase in Hadley circulation in the latitude belt 5°S–10°N and a decrease in the belt 10°–30°N. The precipitation change for 5X in Fig. 5a further reveals the associated shift in the

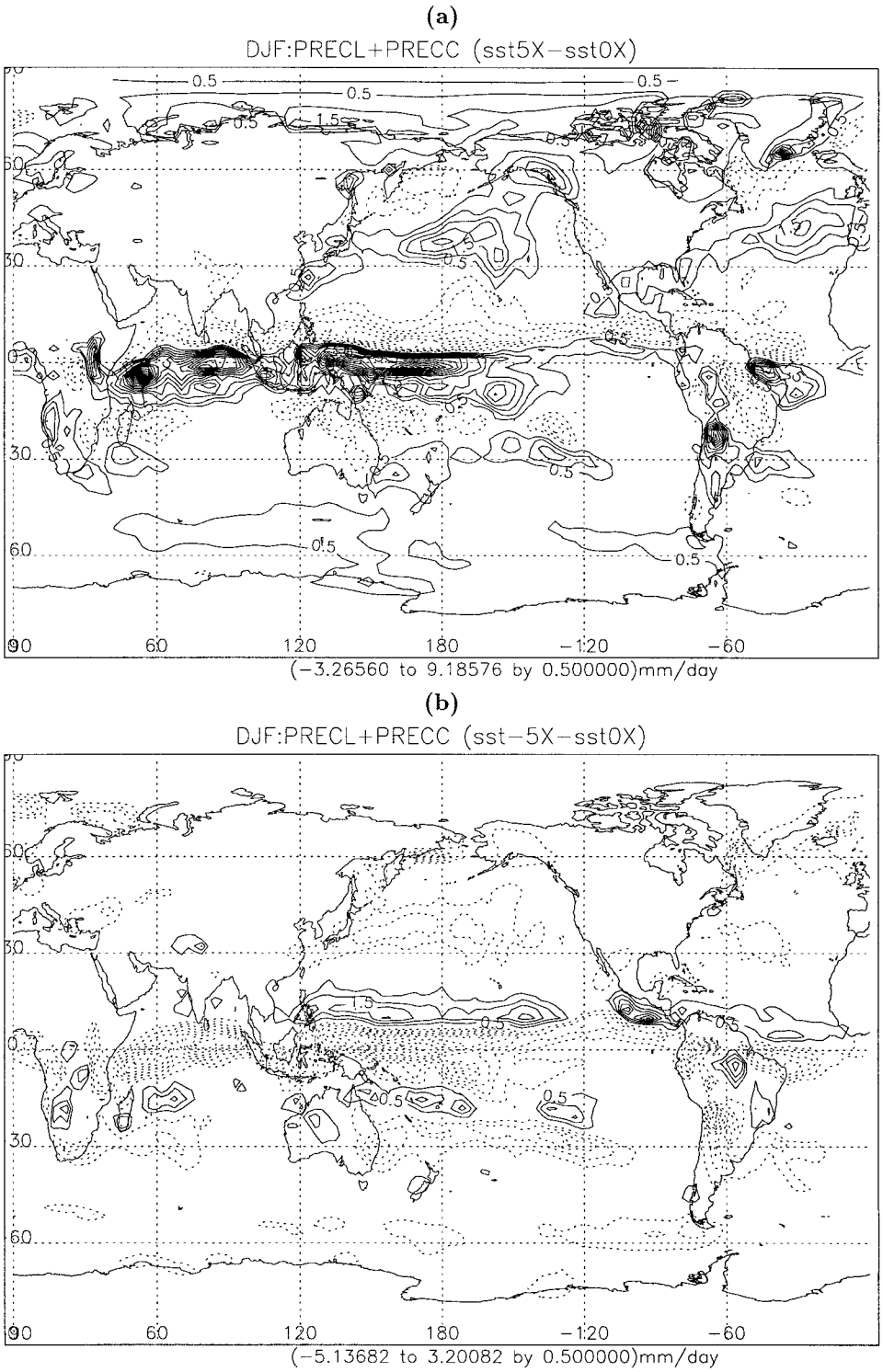

FIG. 5. DJF-mean response in rainfall (mm day^{-1}). Negative contours are dashed. Contour interval is 0.5. The zero contour has been omitted. (a) 5X–0X. (b) −5X–0X.

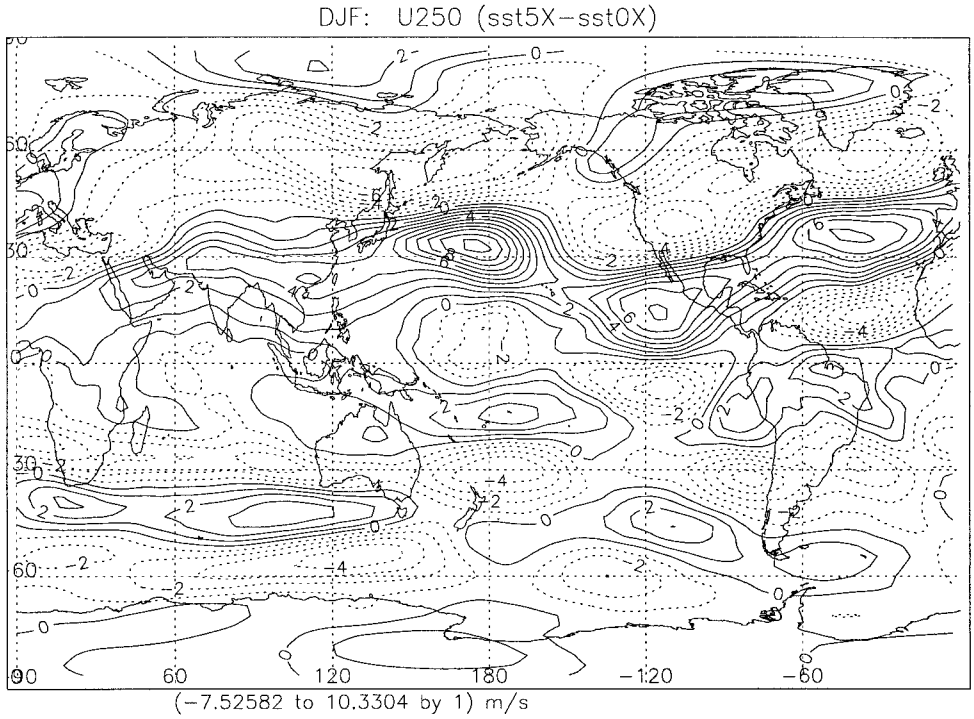

FIG. 6. DJF-mean response for 5X in 250-hPa zonal wind (m s^{-1}). Negative contours are dashed. Contour interval is 1.

ITCZ. Both 5X and 9X (not shown) show a substantial increase in precipitation in equatorial regions, and a corresponding southward shift of the ITCZ, stretching from the Indian Ocean eastward over the equatorial Pacific with a strong signal at the same latitudes in the tropical Atlantic. In MS99 we saw signatures of this response in the vertical energy fluxes at the top of the atmosphere. Furthermore, the vertical distribution of radiative heating confirms the dramatic increase of deep convection in the 10°S–5°N latitude band for these two cases. With the warmer tropical SSTs, CCM3 clearly abandons its bias to place the ITCZ in the NH. This pattern of change in precipitation looks almost reversed (with less magnitude) for −5X in Fig. 5b, which moves the precipitation maximum farther north of the equator than for the control, with a significant decrease in precipitation in the equatorial Pacific. Note that the increase and shift in the Hadley circulation in the warming experiments is also consistent with the equatorward strengthening of the subtropical jet that is depicted in Fig. 4b for 5X.

There are secondary precipitation maxima over the extratropical ocean basins corresponding to the NH storm tracks. The deviation field for 5X, depicted in Fig. 5a, shows maxima stretching downstream of the 0X precipitation maximum in each storm track. There are interesting opposite anomalies in precipitation at NH extratropical latitudes in both ocean basins for 5X and 9X (not shown), with positive deviations to the east and smaller negative ones to the west. The −5X case in Fig. 5b shows a weaker precipitation deviation field, with generally reduced precipitation in the storm-track regions. Thus, by the measure of precipitation rate, the storm-track activity strengthens downstream with a decreased SST gradient (and thus decreased low-level baroclinity), which is, however, accompanied by an overall increase in SST and thus a moister atmosphere. The reversed conclusion is reached when the SST gradient is increased, accompanied by an overall reduction in SST. This result will be examined further in the next section where I shall concentrate on the response in the midlatitude circulation.

b. A closer look at the extratropical response

The extratropical dynamical features of the response for the different cases may be presented as deviations from the eddy geopotential field (geopotential with the zonal average removed) at certain pressure levels of the control simulation. The response is predominantly equivalent barotropic with largest amplitude at tropopause level. In what follows I shall therefore concentrate on the dynamical response at 250 hPa, combined with temperature and the transient eddy heat flux response at 700 hPa, and moisture and the transient eddy moisture flux response at 850 hPa.

The response in the 250-hPa zonal wind is presented in Fig. 6 for 5X. Aside from the strengthening and equa-

torward displacement of the subtropical jet for 5X that was evident in Fig. 4b and can be seen especially over the Pacific, there is a clear longitudinal structure to the response. This is further revealed in the response of the mean eddy streamfunction (the mean streamfunction with the zonal average removed, denoted by $\overline{\psi^*}$) in Fig. 7a for 5X and Fig. 7b for −5X. The extratropical 5X response in this field shows substantial strengthening in many features of the stationary wave field as shown for 0X in Fig. 2b. With regard to the two NH ocean basins, note in particular the amplification of the downstream features in the stationary wave field and the weakening of the poleward features, upstream. Conversely, the −5X response is considerably weaker. When comparing this field for the different cases with a positive trend factor, namely 1X and 9X (not shown) as well as 5X, the close correspondence between the different experiments is striking. It is almost as if the change in stationary waves shows a linear response, when the trend factor is positive. I calculated the pattern correlations between the response in $\overline{\psi^*}$ for these experiments and got values of 0.85 for 9X and 5X deviations and 0.65 for 5X and 1X deviations; both values are quite significant. On the other hand, the pattern correlation of stationary-wave response of −5X with the stationary response of the experiments with a positive trend factor was small. The results are displayed in Table 2.

The storm tracks as depicted by the high-pass-filtered 250-hPa streamfunction variance are shown for 5X and −5X in Figs. 8a,b, respectively. As compared with the storm tracks for 0X in Fig. 2c, the 5X case in the Pacific shows substantial downstream amplification. A downstream shift in storm-track activity over the mid-Pacific in the exit region of the jet is also apparent. Over the Atlantic the 5X case in Fig. 8a shows a decrease in storm-track activity at the beginning of the storm track and a downstream amplification. The response as seen in this dynamic field is thus consistent with the change in precipitation in the storm-track regions, depicted in Fig. 5a. For the −5X case in Fig. 8b, the main difference from the 0X case is a downstream amplification of the Pacific storm track in the exit region of the jet. Elsewhere, the storm tracks for −5X are mostly weaker.

As we saw in section 3a and has been noted in other GCM studies where SST is raised (e.g., Thuburn and Craig 1997), the experiments with a positive trend factor lead to a general warming and expansion of the entire troposphere. It is therefore of interest to see whether an upward shift can be detected in the storm tracks in response to warmer SSTs with a decreased meridional gradient. Figure 9a shows the meridional cross section of the zonally averaged, high-pass-filtered transient kinetic energy. Figures 9b–d show the difference of that field for 5X, 9X, and −5X, respectively, from the 0X case. The maximum zonally averaged NH storm-track amplitude for 0X is reached at latitude 37°N and at 270 hPa. The 9X maximum in high-pass-filtered zonally averaged transient eddy activity (not shown) shows an upward and poleward shift to 42°N and 250 hPa. The pattern of change for the 5X case (in Fig. 9b) is very similar to that for 9X (in Fig. 9c), only the amplitude of change is smaller. Note that for both of these cases, throughout most of the troposphere, the zonally averaged transient kinetic energy is decreased. Thus, the 250-hPa signature of increased activity at the downstream end of the storm tracks, at least in the zonal mean, is only detected in the upper troposphere, between 40° and 55°N. However, it should be noted that the positive trend-factor experiments showed a decrease in streamfunction variance at the upstream end of the storm tracks that would contribute to a weaker zonally averaged signal. There is an increase in transient kinetic energy in the low-latitude high troposphere. This is again consistent with the increased convective activity at low latitudes. For −5X, shown in Fig. 9d, there is upper-level decrease in transient kinetic energy, but very little change elsewhere in the NH.

We have yet to examine the baroclinic signature of the response. The contours in Fig. 10a represent the 700-hPa temperature distribution and the arrows the high-pass transient heat flux ($\overline{\mathbf{v}'T'}$), for the control case 0X. Note that over the Atlantic, the maximum heat flux is clearly over the western part of the ocean basin. The response both in terms of temperature and transient heat flux in the positive trend-factor cases is quite similar in pattern. The response for −5X is considerably less pronounced, consistent with the weaker response in streamfunction variance in that case. I chose to show only the response in the 5X case in Fig. 10b. For clarity, the fields in Fig. 10 have been smoothed to T21 horizontal resolution.

At 700 hPa the warming signal is stronger over the continents at about 40°N, resulting in a minimum thermal anomaly centered over each ocean basin for the cases with a positive trend factor. At upper levels there is no such structure to the thermal response; rather it has a zonal signature. In all the positive trend-factor cases there is strong convergence of transient heat flux into the minimum thermal anomaly, which shows that the transient eddies are not maintaining this feature; rather it is the mean flow. The thermal response is particularly interesting for these cases over the Pacific, where in addition to the minimum thermal anomaly over the central basin there is a relative maximum anomaly downstream. This sets up a strong northward heat flux between the two anomalies, which acts to feed the strong secondary Pacific storm-track maximum in the 5X (Fig. 8a) and 9X (not shown) experiments. The response in terms of transient heat flux over the Pacific is divergence over the east, followed by convergence over the central basin reaching north and east, followed by divergence to the west. Again, the pattern of heat flux convergence/divergence (not shown) is remarkably similar between the experiments with a positive trend factor, almost as if it were linear. The Atlantic is a narrower ocean basin that only has one thermal anomaly. The positive trend-

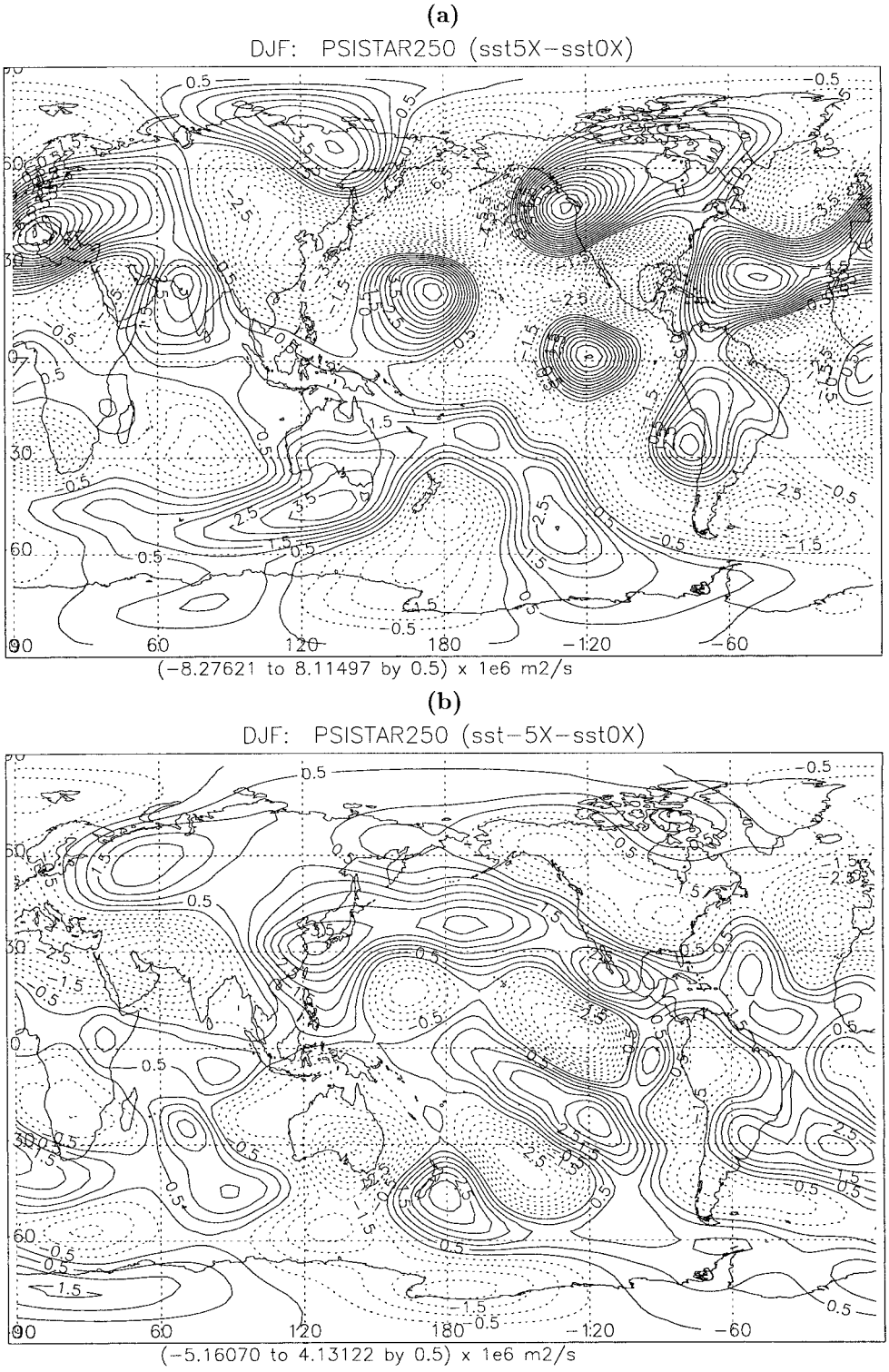

FIG. 7. DJF-mean response in eddy streamfunction (mean streamfunction with zonal average removed) on the 250-hPa surface (10^6 m^2 s^{-1}). Negative contours are dashed. Contour interval is 0.5. (a) 5X–0X. (b) −5X–0X.

TABLE 2. DJF pattern correlations.

$\Delta\overline{\Psi^*}$	1X	5X	9X
5X	0.651 180		
9X	0.543 274	0.845 387	
−5X	−0.021 947 5	−0.335 186	−0.370 028

factor experiments have strongly reduced heat flux in the western North Atlantic north of 40°N.

In Fig. 11a I include the effects of moisture for 0X. The contours represent specific humidity and the arrows show transient eddy moisture flux, both at 850 hPa where the flux has a maximum. North of the subtropics, there is strong resemblance between this figure and that of the temperature and heat flux, shown in Fig. 10a. However, the moisture field is dominated by the low-latitude distribution. In Fig. 11b we consider the moisture response and the transient moisture flux at 850 hPa, smoothed to T21 resolution, for 5X. In the cases with a positive trend factor, there is greatly increased specific humidity at low latitudes associated with the nonlinear dependence of saturation vapor pressure on temperature. For −5X the response is considerably weaker. For 5X and 9X (not shown), a tongue of moist air stretches into the central North Pacific from the Tropics, and associated with it is an increased northward transient moisture flux. The increased flux converges in the area just upstream of increased storm-track activity as seen in the field for $\overline{\psi'^2}$ at 250 hPa. In the eastern North Atlantic a moist anomaly in 5X and 9X is again associated with an increased northward transient moisture flux that is just upstream of the increased storm-track activity as seen in $\overline{\psi'^2}$. The downstream strengthening of the storm tracks at upper levels therefore has a signature of increased latent heating and increased transient moisture flux at lower levels.

To summarize this section, the upper-tropospheric response in the positive trend-factor cases is characterized by greatly increased stationary waves, particularly over the ocean basins, increased storm-track activity at 250 hPa toward the rear of the storm tracks, with decreased activity toward their front end. There is remarkable correspondence in the response fields for these cases in terms of the amplitude of trend factor, especially for the stationary waves. With the decreased low-level baroclinity, the positive trend-factor cases have less zonally averaged eddy kinetic energy over most of the troposphere. Only close to tropopause levels is there an increse in this quantity, corresponding to the general expansion of the troposphere. The low-level transient eddy fluxes of heat and moisture show a response that is in close correspondence in the different positive trend-factor cases. The response in these quantities is different in the two ocean basins. This is related to the more extensive area of the Pacific as compared with the Atlantic.

4. The JJA-mean SH response

There are several quite pronounced differences between the geography of the two hemispheres that lead to different atmospheric circulation patterns. The SH is primarily ocean covered, resulting in considerably less excitation of stationary wave activity than in the NH. The extensive area of the Antarctic Circumpolar Current, which passes at its narrowest point through Drake Passage, has no land surface. Midlatitude storm activity tends to be more continuous in longitude in the SH than in the winter NH. Because of the extensive high-latitude ocean area, the fictitious sea-ice change accompanying the change in SST (that was discussed in section 2a) will be more pronounced in the SH. Results at high latitudes should be interpreted with that in mind. The asymmetry in land (and its elevation) versus ocean area between low latitudes of the two hemispheres also contributes to a stronger winter Hadley circulation in the SH winter (JJA). This is the time of intense monsoonal flow in the NH. Last, the SH contains an extensive and high continent at the Pole that reaches the Antarctic circle along a wide stretch. Antarctica represents a heat sink throughout the year and sets up a baroclinic zone that remains strong even in summer. Trenberth (1991) has analyzed several years of European Centre for Medium-Range Weather Forecasts data to depict the SH storm tracks.

a. Main features of the response

Let us first concentrate on zonally averaged fields of temperature, zonal wind, moisture, and mean mass streamfunction and their response to the forcing in the meridional plane. As in the NH, overall the response is quite linear in the trend factor. Moreover, the response in temperature is similar to the DJF NH response, except the midlatitude stratospheric cooling for a positive trend factor is more pronounced in this case. The mean meridional circulation is stronger in JJA in the SH than in DJF in the NH. This applies both to the winter Hadley circulation and the midlatitude indirect circulation. The zonally averaged jet in the JJA-averaged SH, is stronger than its NH winter counterpart, with a double-jet structure and the poleward maximum extending into the stratosphere. The response in $[\overline{u}]$ for 5X shown in Fig. 12a is considerably stronger than that in NH DJF. There is a strong shear zone in the response around tropopause level at 30°S, where the strongest gradient in the temperature response is located.

The response in mass streamfunction, shown for 5X in Fig. 12b, is different from the DJF response. Now, the winter Hadley circulation is decreased everywhere. (In the SH the mass streamfunction for the winter Hadley circulation is negative.) This weakening of the Hadley circulation is due in part to the decreased temperature difference between ocean and continents in the NH Tropics, where the upward branch of the Hadley

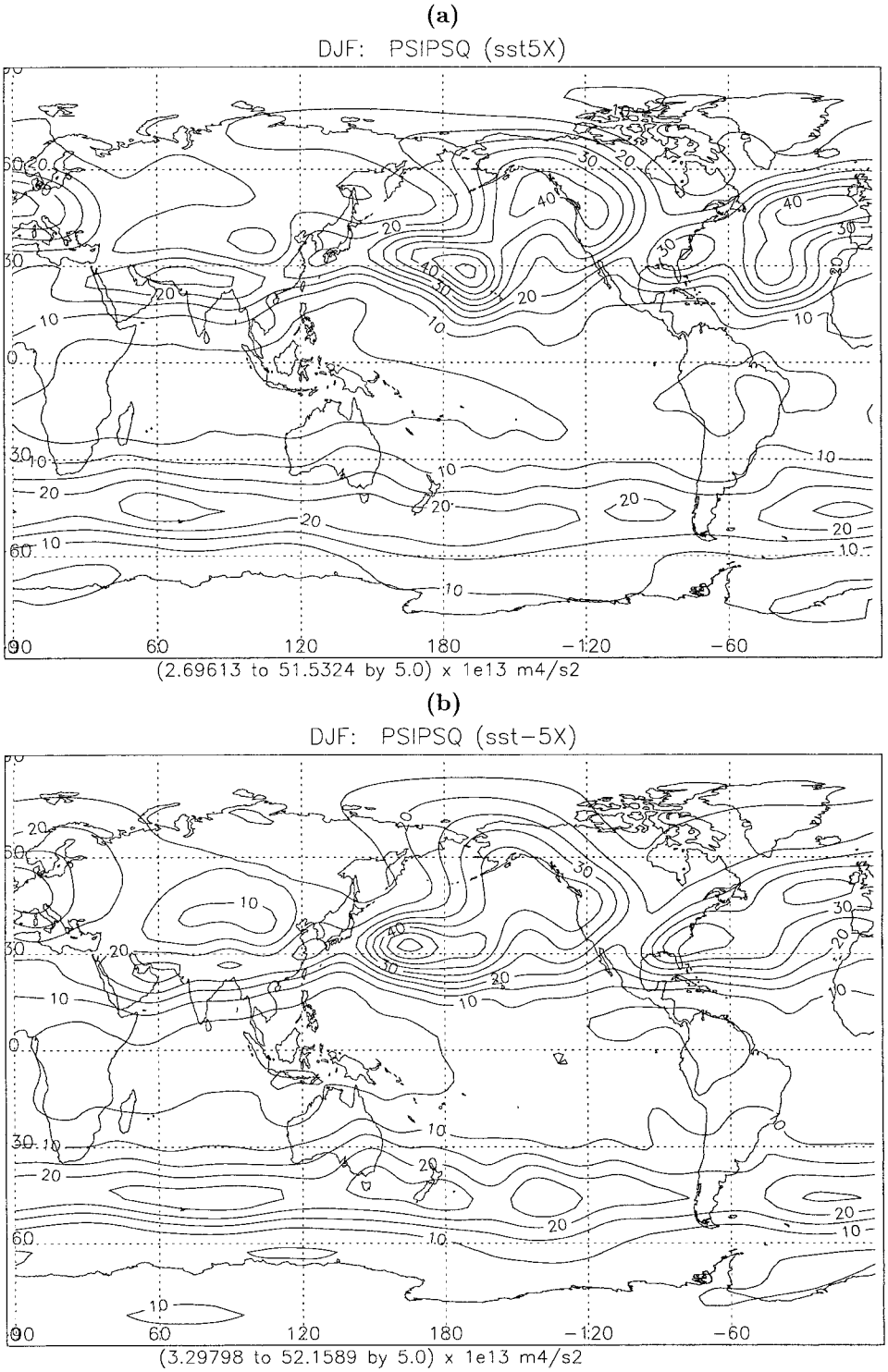

FIG. 8. DJF-mean high-frequency filtered transient eddy streamfunction variance (10^{13} m^4 s^{-2}). Contour interval is 5. (a) 5X. (b) −5X.

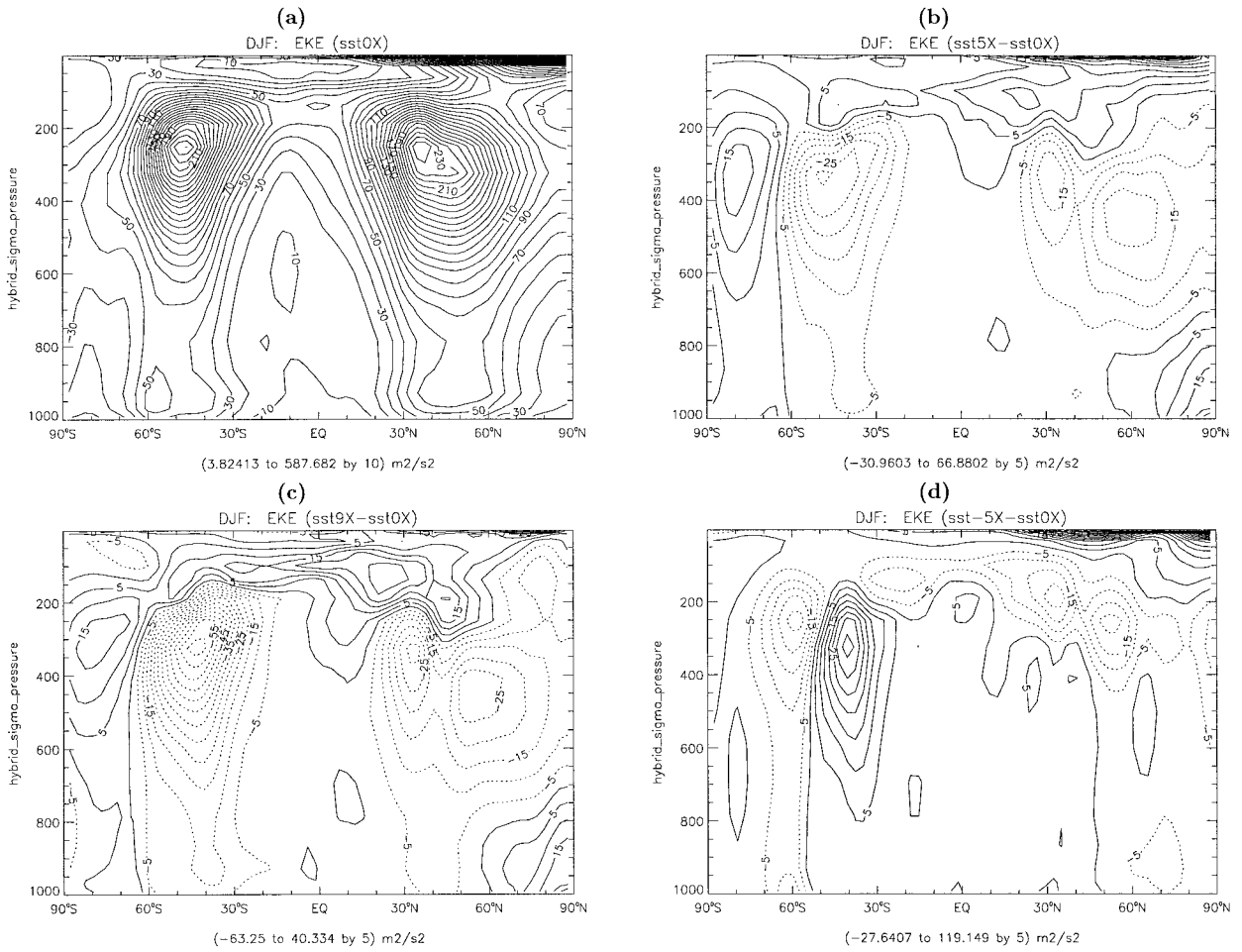

FIG. 9. DJF-mean, zonally averaged, high-frequency filtered, transient eddy kinetic energy in the meridional plane ($m^2\ s^{-2}$). Negative contours are dashed. (a) 0X. Contour interval is 10. (b) 5X–0X. Contour interval is 5. (c) 9X–0X. Contour interval is 5. (d) −5X–0X. Contour interval is 5.

circulation is located. This results in weakened monsoonal flow.

The response in terms of precipitation is shown for 5X in Fig. 13. Consistent with the change in low-latitude mean meridional circulation, extensive areas in the tropical NH show reduced precipitation. Note in particular the substantial decrease in precipitation in the area of the Asian summer monsoon. Now the increase in tropical precipitation in a warmer and thus moister world takes place for the most part over the equatorial Pacific and in the SH. In the extratropical SH, precipitation increases east of South Africa in the Indian Ocean and west of Chile over the east Pacific. Precipitation also increases along the Antarctic coastline, corresponding to a shift of the baroclinic zone (arising from the sea-ice edge in 0X) to the coastline.

The low-latitude response for −5X (not shown), both in zonally averaged mass streamfunction and precipitation, exhibits remarkably similar characteristics to the 5X response, only of opposite sign. In this case the Hadley circulation is stronger and the Asian summer monsoon is more vigorous in many places, as shown by a larger precipitation rate than for 0X. There is decreased precipitation over the equatorial Pacific. Even though the patterns of precipitation change remain quite close in the extratropics, the amplitude of change is less for −5X than 5X. This is not surprising in light of the strong dependence of saturation water vapor pressure on temperature.

b. A closer look at the extratropical response

In the NH winter extratropics, it is found that for many of the fields the response for a positive trend factor was quite linear between experiments, whereas for the negative trend-factor case the response behaved differently. In contrast, in the SH winter extratropics the response is quite linear, irrespective of the sign of the trend factor. I attribute this simpler behavior in the SH extratropics at least in part to the simpler land–sea distribution and thus much smaller amplitude stationary waves. Here, I shall only consider the response in one

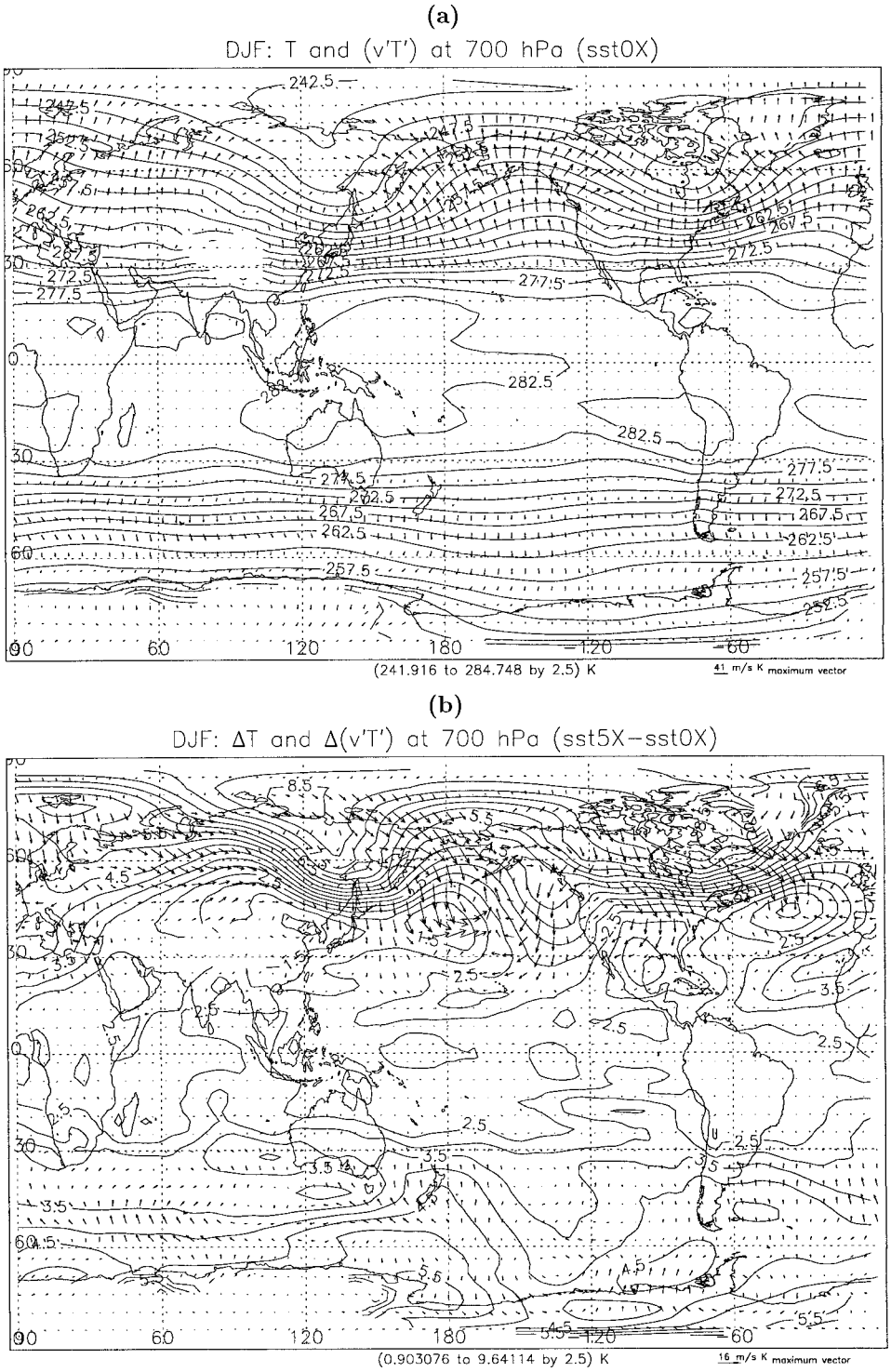

FIG. 10. DJF-mean fields on the 700-hPa surface, smoothed to T21 horizontal resolution. (a) 0X temperature (contour interval is 2.5 K) and high-frequency filtered transient temperature flux [vectors (m K s^{-1})]. Vector, shown in lower-right-hand corner, has the value 41. (b) The 5X temperature response [contours (K), contour interval is 0.5], and response of high-frequency filtered transient temperature flux [(vectors (m K s^{-1})], vector has value 16.

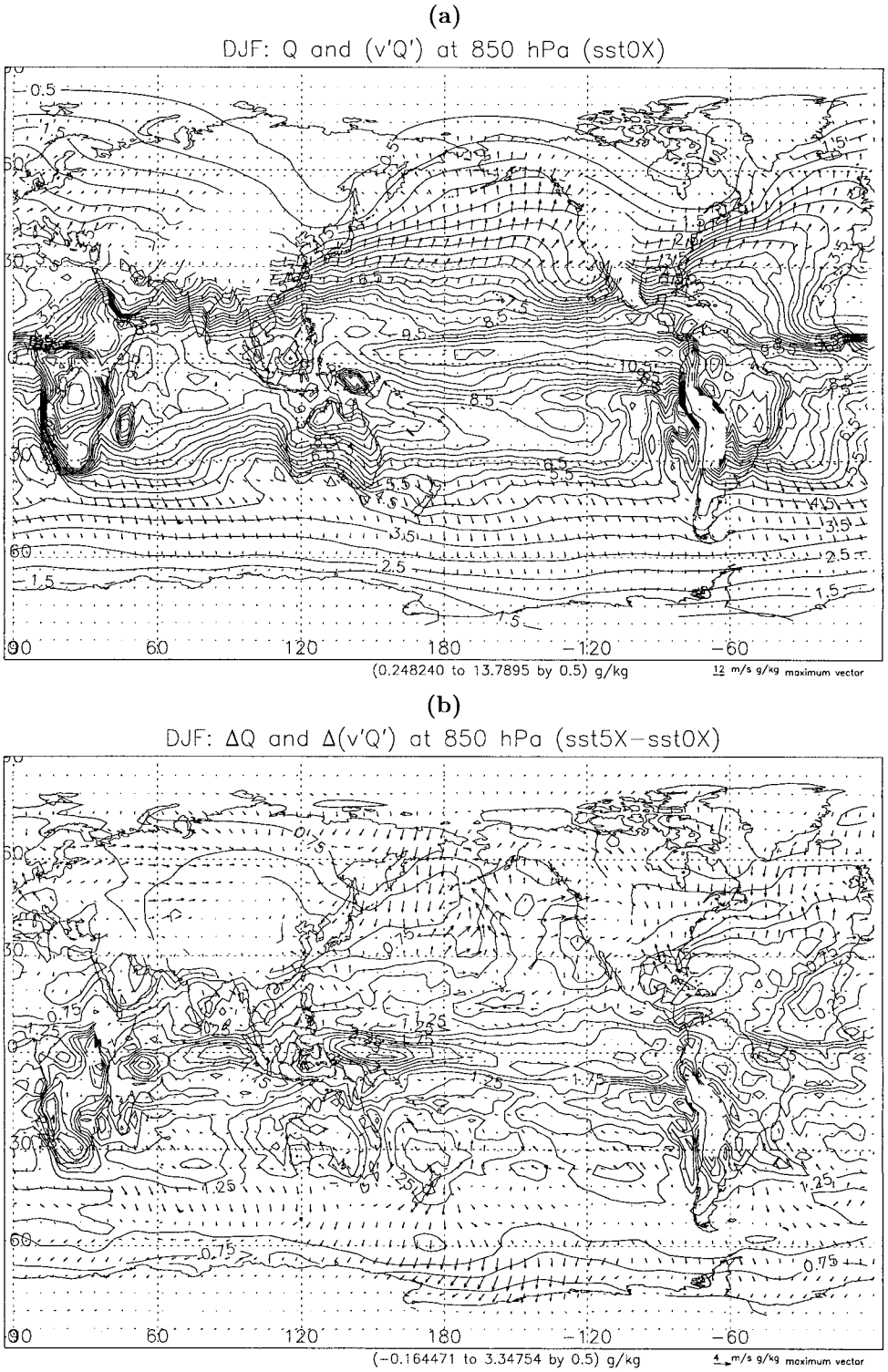

FIG. 11. DJF-mean fields on the 850-hPa surface, smoothed to T21 horizontal resolution. (a) 0X specific humidity [contours (g kg^{-1}), contour interval is 0.5], and high-frequency filtered transient moisture flux [vectors (m g kg^{-1} s^{-1})]. Vector, shown in lower-right-hand corner, has the value 12. (b) 5X response in specific humidity [contours (m g kg^{-1} s^{-1}), contour interval is 0.25] and response of high-frequency filtered transient moisture flux [vectors (m g s^{-1} kg^{-1}), vector has value 4].

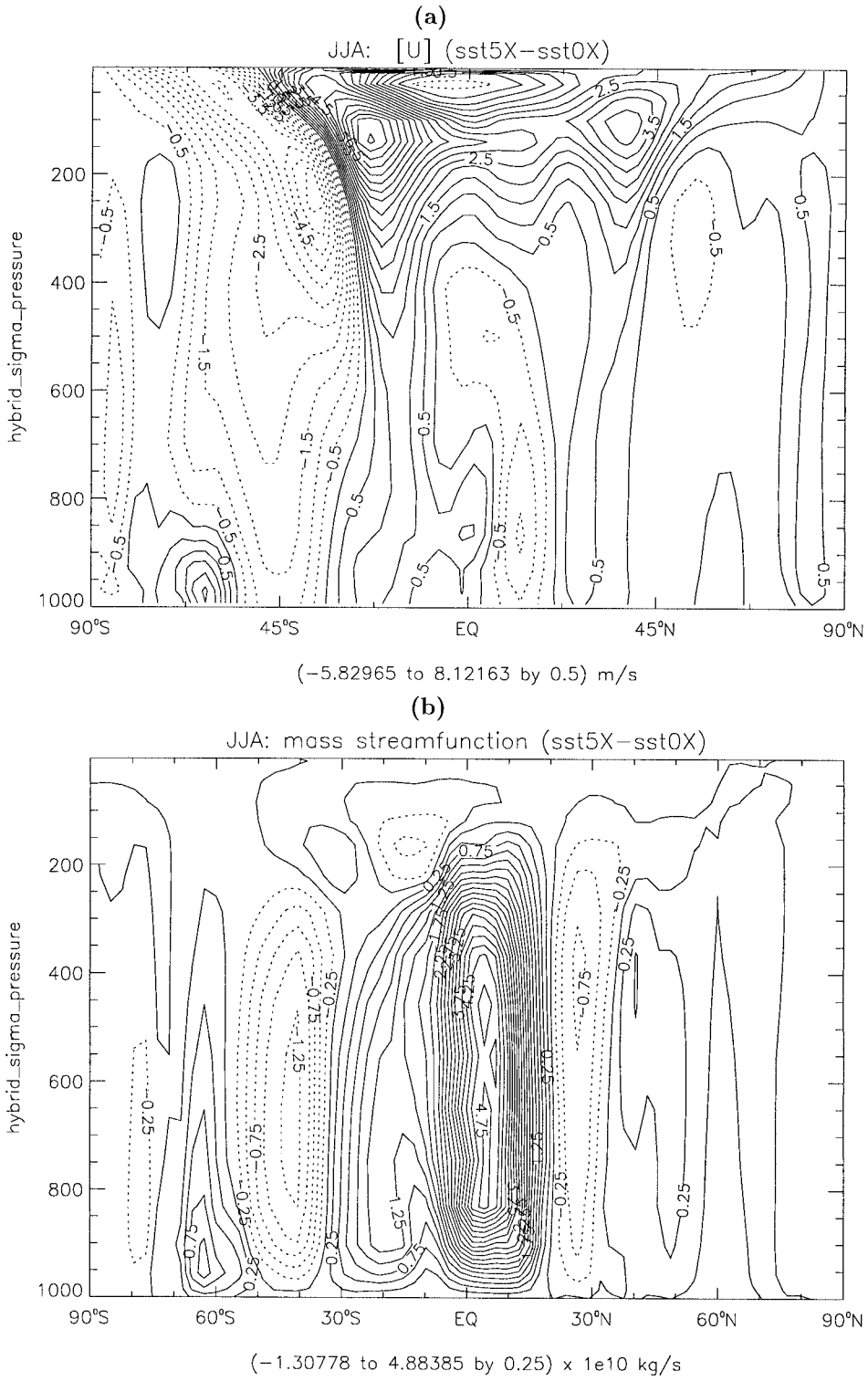

FIG. 12. JJA-mean, zonally averaged response for 5X (deviations from 0X). Negative contours are dashed. (a) Zonal wind (m s^{-1}), contour interval is 0.5. (b) Mass streamfunction [(10^{10} kg s^{-1}), contour interval is 0.25].

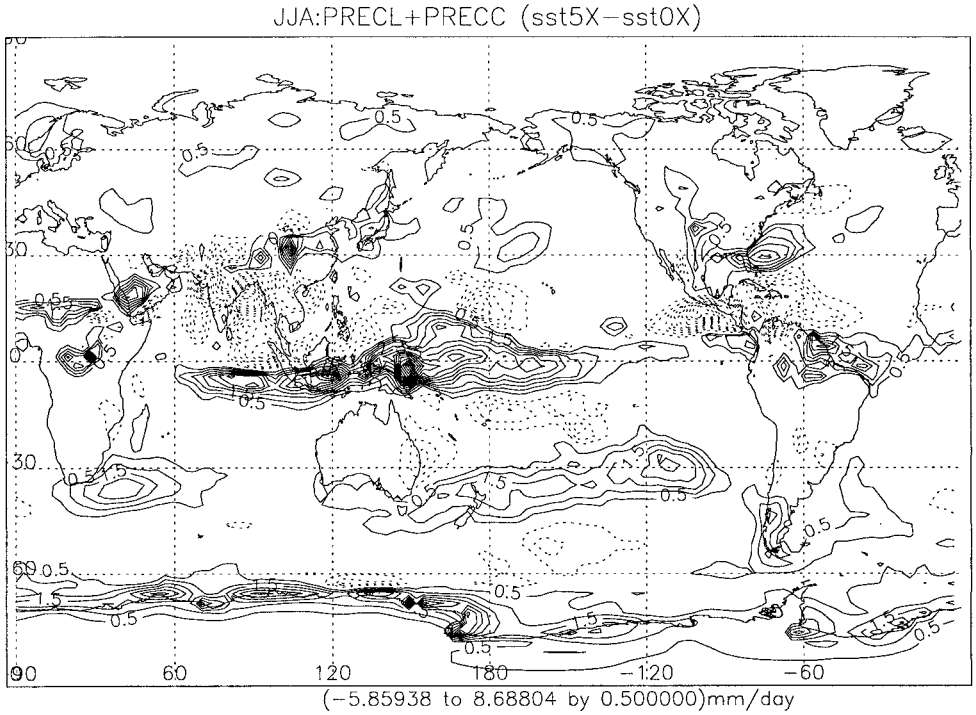

FIG. 13. JJA-mean response in rainfall for 5X (mm day^{-1}). Negative contours are dashed. Contour interval is 0.5. Zero contour has been omitted.

case, that of −5X. The choice of −5X was in part made because of the substantial increase in poleward heat transport in that case that was a result of changes both in the vertically integrated and zonally averaged transient eddy part as well as the mean meridional circulation as seen in Fig. 12 of MS99.

Let us first examine the response at 250 hPa. Figure 14a shows the mean JJA zonal wind for 0X and Fig. 14b shows the response in this field for −5X. The largest response is in the Pacific, corresponding to a weakening and poleward shift of the subtropical jet east of Australia. This is upstream of the area of maximum storm-track activity for 0X as seen in the variance of the high-frequency streamfunction, shown in Fig. 15a. The response in the storm track for −5X is shown in Fig. 15b. Note the increase in amplitude and the poleward shift in the Pacific part of the storm track. A secondary area of storm-track amplification is downstream of the other maximum of storm-track activity in the SH, south of Africa. The question arises whether transient eddy forcing is affecting the change in zonal wind seen in Fig. 14b. As seen in Fig. 16a, which depicts the change in the quantity $\overline{S}$ that was discussed in section 2b, there is indeed close correspondence between the change in the jet, both in the Pacific and in the Indian Ocean, and the change in barotropic forcing by the transients. Thus there appears to be a transient eddy feedback on the mean flow. The response in terms of transient heat flux at 700 hPa is shown in Fig. 16b. The increase in heat flux for −5X is located upstream of the maximum increase in $\overline{\psi'^2}$ in both locations. The increase in low-level heat flux is therefore consistent with the increase in upper-level storm-track amplitude. The contours in Fig. 16b represent the negative of the 700-hPa temperature deviation of −5X from 0X.

To get a better picture of the vertical storm-track structure in this case and the other cases, I again examine the response in time-filtered, zonally averaged transient kinetic energy in the meridional plane. The results are shown in Fig. 17d for the response in the −5X case. It shows an increase in this quantity almost throughout the entire SH midlatitude troposphere. There is an opposite signal for 5X and 9X in Figs. 17b,c, showing decreased eddy kinetic energy almost throughout the midlatitude troposphere. For comparison, we show the zonally averaged transient kinetic energy for 0X in Fig. 17a. The response is remarkably consistent between the different experiments. Note that the response in the same quantity for the NH winter was different for the case with a negative trend factor from the cases with positive trend factors.

The high-latitude response is hard to interpret because of the somewhat arbitrary shift in sea ice that was discussed earlier. The decrease in transient kinetic energy for −5X, stretching from high latitudes to approximately 57°S is due to the sea-ice edge moving northward by about 5° latitude, thereby cutting off surface fluxes. Similarly, the sea-ice edge moves to the coastline of Antarctica in the warming cases, resulting in an increase in transient kinetic energy at high latitudes for those

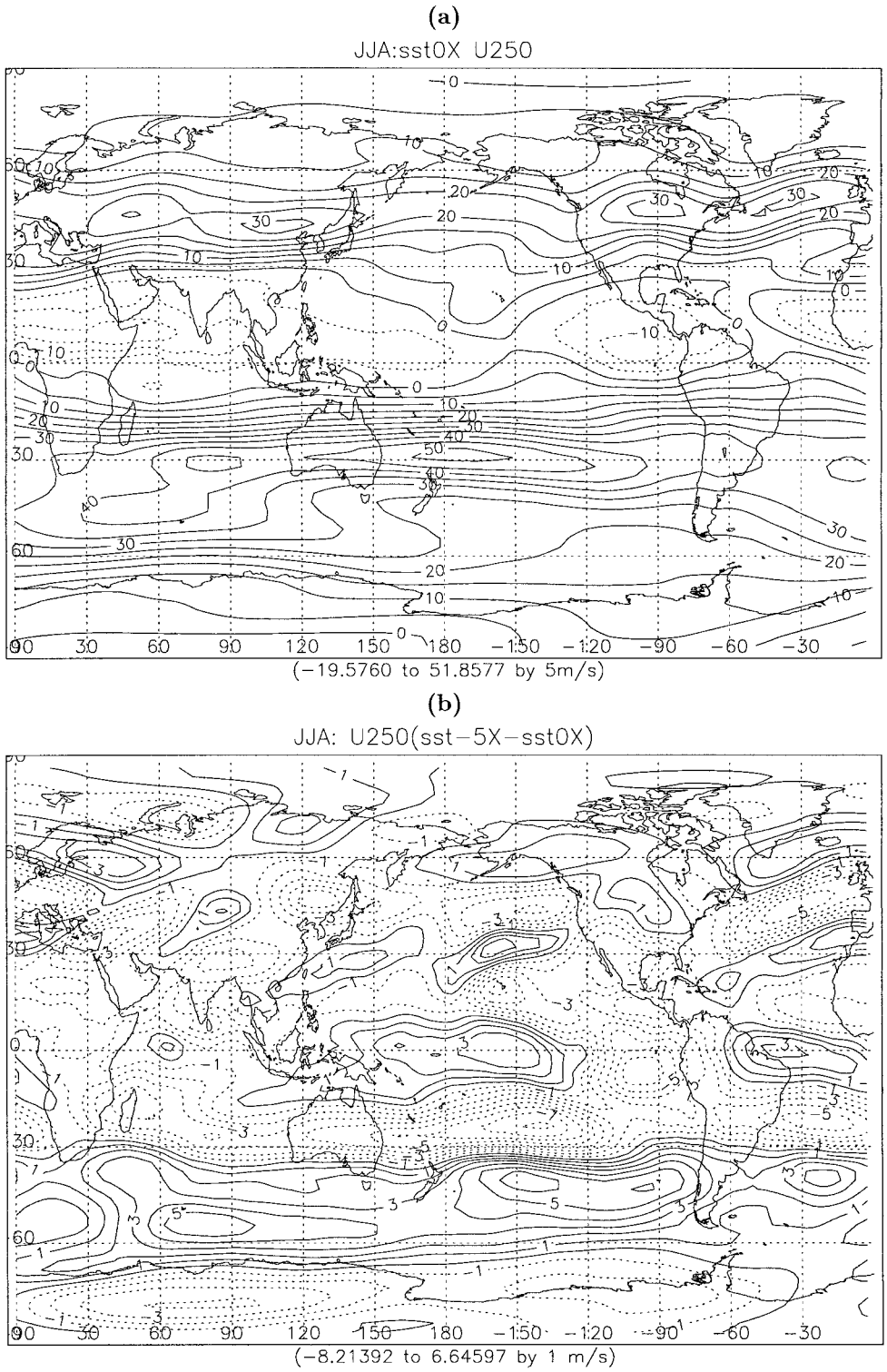

FIG. 14. JJA-mean fields on the 250-hPa surface. (a) 0X zonal wind (m s^{-1}). Contour interval is 5. (b) −5X response in zonal wind (m s^{-1}). Contour interval is 1, negative contours are dashed.

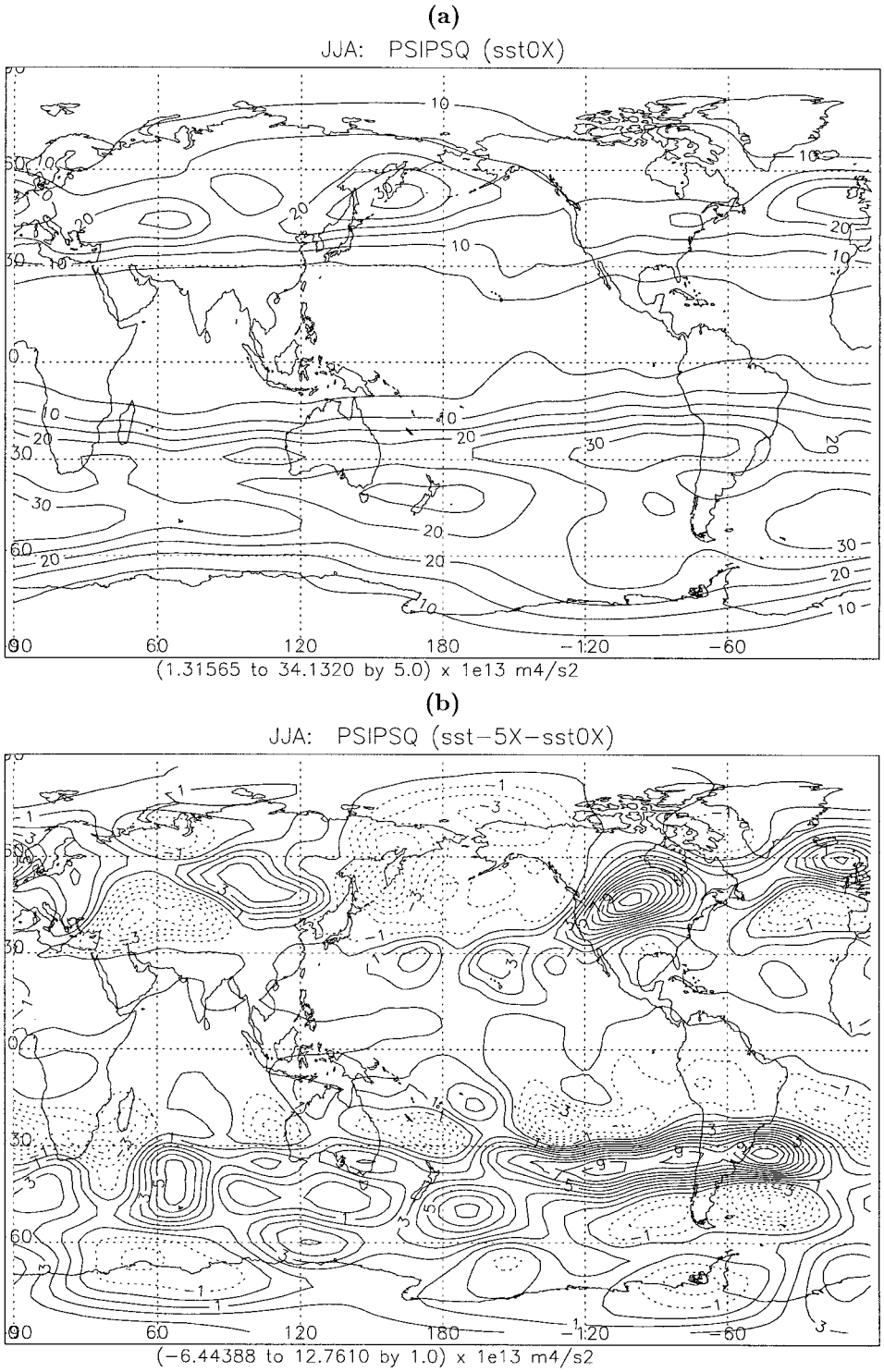

FIG. 15. JJA-mean fields on the 250-hPa surface. (a) 0X transient eddy streamfunction variance (10^{13} m^4 s^{-2}). Contour interval is 5. (b) −5X response of transient eddy streamfunction variance (10^{13} m^4 s^{-2}). Negative contours are dashed. Contour interval is 1.

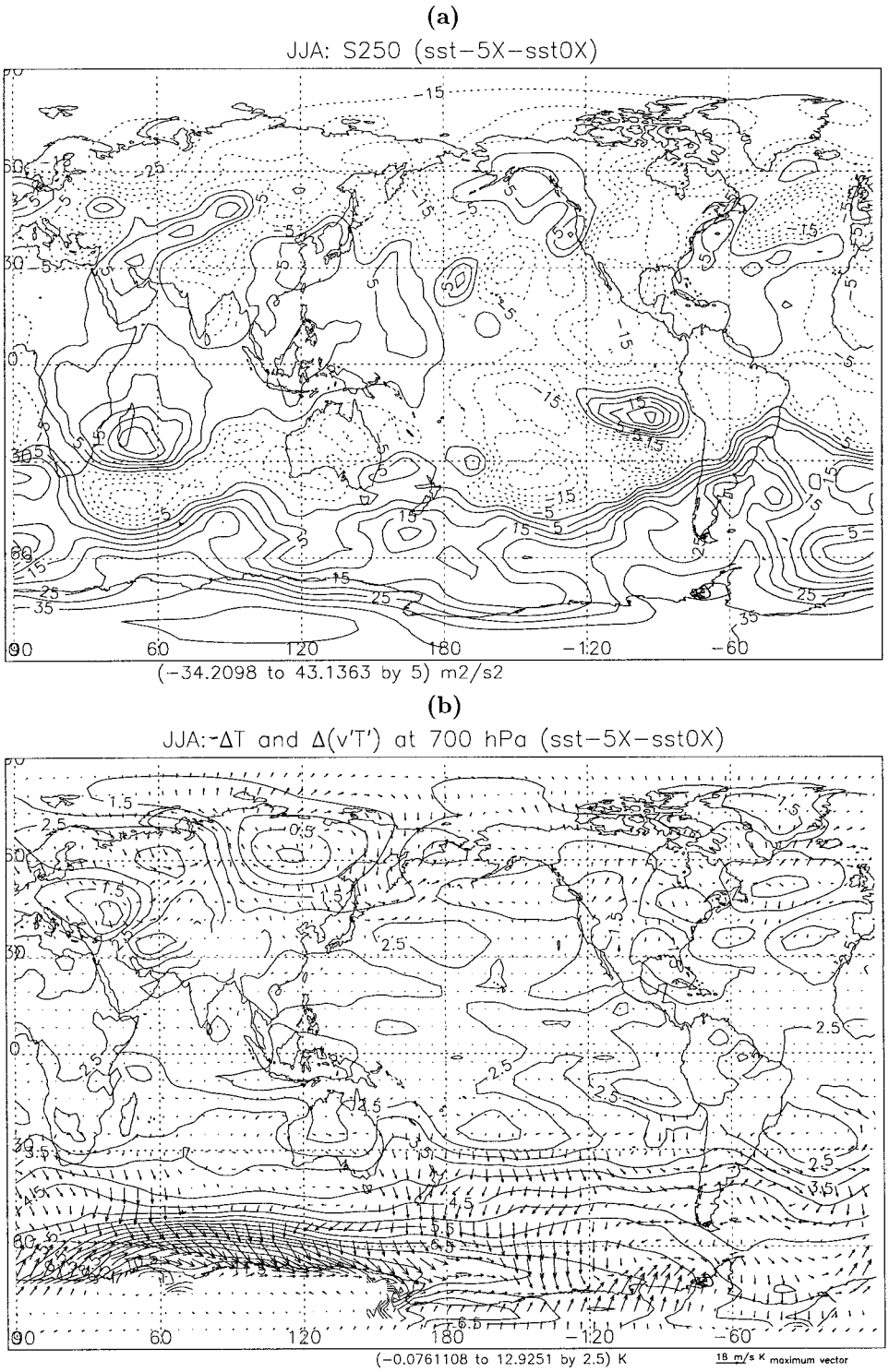

FIG. 16. JJA-mean response of −5X. (a) Response of the barotropic forcing of the mean streamfunction by the high-frequency transient eddies at 250 hPa ($m^2\ s^{-2}$). Contour interval is 5. Negative contours are dashed. (b) The negative of the 700-hPa temperature response [contours (K), contour interval is 0.5], and response of high-frequency filtered transient temperature flux [vectors (m K s^{-1})] at the same level, smoothed to T21 horizontal resolution. Vector in lower-right-hand corner is 18.

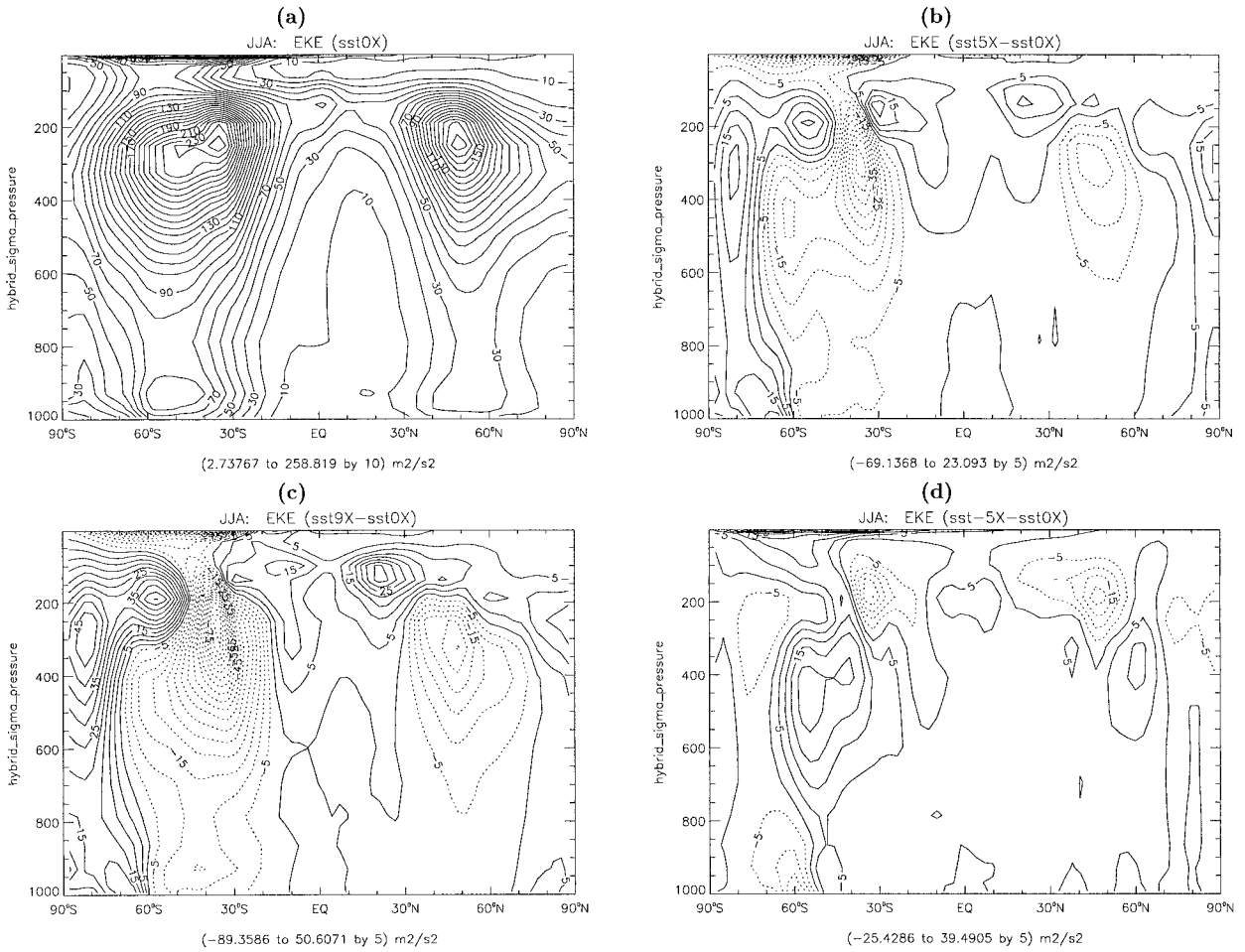

FIG. 17. JJA-mean, zonally averaged, high-frequency filtered, transient eddy kinetic energy in the meridional plane ($m^2\ s^{-2}$). (a) 0X. Contour interval is 10. (b) 5X–0X. Negative contours are dashed. Contour interval is 5. (c) 9X–0X. Negative contours are dashed. Contour interval is 5. (d) −5X–0X. Negative contours are dashed. Contour interval is 5.

cases. It would be interesting to repeat these experiments while holding sea ice fixed.

5. Concluding remarks

I have examined the response of the mean winter circulation in each hemisphere to zonally averaged SST anomalies that have doubled amplitude at high latitudes as compared with low latitudes. The SST was changed by adding or subtracting a multiple of a meridional profile of SST change, which is based on the centennial trend in the annual and zonal average of SST data. We use the term ''trend factor'' to refer to the factor by which the centennial SST trend is multiplied before adding it to the climatological SST.

The picture that emerges from the numerical experiments is that the response of the NH extratropical winter circulation to a positive trend factor of SSTs is remarkably consistent in many fields. It is almost as if the response is linear in the NH stationary-wave and zonal-wind response. Even the transient eddy variance and covariance fields show close correspondence for the positive trend-factor cases. The response of the circulation to the cooling of SST, where the trend factor is negative, behaves differently and is considerably weaker.

There is asymmetry in the response between the two hemispheres in that the SH response is strikingly consistent between experiments irrespective of the sign in the trend factor. I attribute the different behavior in the NH at least in part to its strong stationary-wave response. In a diagnostic study such as this one, it is difficult to determine mechanisms. In order to determine the forcing of the NH strong stationary-wave response in these experiments, one would need a linear model consistent with the CCM3. To my knowledge, such a model has not been developed. It is beyond the scope of the current study to develop such a model. It is noted here that such a linear model would be very useful since the CCM3 is widely used as a community climate model.

One can still speculate on forcing mechanisms of the

stationary-wave response in the positive trend-factor experiments. The most obvious candidate is increased temperature contrast between the cold continents of winter and the relatively warm SST. However, in the latitude band 45°–55°N, the zonally averaged surface temperature over land only warms more than that over ocean only. Even when considering the response in surface temperature only over the east coast of the two continents, the zonal contrast in surface temperature has decreased in midlatitudes and north thereof. From Fig. 10d in MS99, there is greatly increased heat transport due to stationary waves for both 5X and 9X in the latitude band 30°–60°N. Other possible forcing mechanisms are as follows: 1) diabatic heating in the Tropics and midlatitudes, 2) change in low-level winds and thus forcing due to orography, and 3) transient eddy forcing. The response in rainfall is quite pronounced (especially at low latitudes) so I speculate that the first one above is due to be important. In fact, the tropical response is quite interesting. This paper has emphasized the extratropical response because the boundary forcing is greatest at high latitudes. I examined the response in low-latitude flow at both the 850- and the 250-hPa surfaces. The response is especially strong in JJA and corresponds both for 5X and 9X to the entire shutdown of the Indian as well as the American monsoonal circulations. By contrast −5X shows enhanced monsoonal flow, corresponding to the enhanced temperature difference between continents and oceans.

Some of the details of the response in the positive trend-factor experiments resemble the response to experiments that have increased greenhouse gas (GG) concentrations. This is not surprising since the atmosphere is heated from below and in the positive trend-factor cases I am using the long-term trends in SST data, which include effects of increased levels of GG concentrations. Since I am exaggerating timescales to get an amplified response, one might think that the response should be stronger. However, even if one assumes that all of the change in SST over the last century was a result of GG warming (which neglects natural variability and is therefore an incorrect assumption), one has to take into account a time delay of warming due to the thermal inertia of the ocean. If one were to assume that the SST warming over 1903–94 is due to a constant increase in CO_2 from the turn of the century to 1975, one gets a growth rate of approximately 0.16% yr^{-1}. This would imply a timescale of doubled CO_2 of about 450 yr, which is much longer than the timescales for global warming scenarios. Admittedly, this is a back-of-the-envelope calculation that neglects all natural variability, but it is close to the 5X timescale. Other studies (e.g., Stephenson and Held 1993; Timbal et al. 1995) have used SST distributions from coupled GCMs with doubled CO_2 to force atmospheric GCMs.

Among the features of the 5X and 9X experiments that resemble global warming experiments is the zonally averaged temperature response. It has the most intense warming taking place in the upper-tropospheric Tropics and in high-latitude surface areas (an effect that gets amplified by the disappearance of sea ice). The result is an increase in baroclinity in the upper troposphere and a decrease at low levels. At the same time, because of the warming of the troposphere, the specific humidity has increased significantly. Note that the negative trend-factor experiment shows the opposite response in terms of zonally averaged temperature and hence moisture content. The question of the effect of greenhouse warming on baroclinic-wave, transient behavior and the storm tracks is thus relevant here. There are two competing processes at work. First is the decrease in low-level baroclinity, which idealized experiments have found to be more important than the increase in upper-level baroclinity (e.g., Pavan 1996, and references therein). Second, the increased moisture content should fuel increased storm-track activity since more latent heat of condensation is available to energize the incipient systems. Pavan et al. (1999) found in baroclinic life cycle experiments with a simple moisture parameterization scheme that increasing low-latitude moisture considerably strengthened development. The experiments indicate an overall weakening of the storm tracks in the positive trend-factor cases, in spite of the increased moisture content. Even the negative trend-factor case shows storm-track weakening in the NH winter, but an increase in storm-track activity in the SH winter. The troposphere expands in the warming experiments, which leads to increased storm-track activity in the uppermost troposphere.

GCM experiments forced by increased concentrations of greenhouse gases have mostly focused on the response of the storm tracks in the NH. In general, their results agree with my results with positive trend factors (e.g., Hall et al. 1994; Ulbrich and Christoph 1999; Carnell et al. 1996; Schubert et al. 1998). Examining the response at the 250-hPa level, I find slightly increased storm-track activity at the downstream end and decreased activity at the upstream end of the NH storm tracks. The increase in moisture fuels the NH storm tracks over the eastern half of both ocean basins (as shown in the increased low-level poleward transient moisture flux from low latitudes), such that both storm tracks exhibit downstream strengthening. Over the northwestern sides of the ocean basins both storm tracks weaken and the weakening is associated with decreased poleward transient heat flux and decreased low-level baroclinity.

The JJA-mean tropical response for the positive trend-factor cases is associated with the weakening of the winter Hadley circulation and substantially decreased NH summer monsoon circulations with increased precipitation over the equatorial west Pacific. The SH midlatitude response is quite zonal in comparison with the DJF-mean response in the NH. The positive trend-factor cases show a weakening of the midlatitude storm track. On the equatorward side of the

storm track, the subtropical jet retreats farther equatorward with the weakened Hadley circulation. Conversely, the negative trend-factor case shows a strengthening of the storm track in midlatitudes, a stronger Hadley circulation that is mostly associated with increased dry static energy transport, and a poleward shift in the subtropical jet. Thus the decrease in low-level baroclinity for the positive trend-factor experiments and increase in low-level baroclinity for the negative trend-factor experiment are playing a greater role in the SH winter response than in the NH winter response.

Last, it should be noted that the climate forcing used in these experiments, that is, the centennial trend in zonally and annually averaged SST as obtained from the GISST2 dataset, is far more reliable in the NH than in the SH. This should be kept in mind when interpreting results for the SH, especially if one is attempting to draw an analogy with global warming scenarios for the positive trend-factor experiments.

Acknowledgments. The author wishes to thank the editor, Jim Hack, R. Saravanan, and an anonymous referee for helpful comments on the manuscript. She thanks Didi Sariyska and Chia-chi Wang for assistance with some of the data analysis. This work was supported by NSF under Grant ATM-9908883 and by NOAA OGP under Grant NA96GP0420. Allocations of computer time were made by the San Diego Supercomputer Center and the Scientific Computing Division of NCAR.

REFERENCES

Carnell, R. E., C. A. Senior, and J. F. B. Mitchell, 1996: An assessment of measures of storminess: simulated changed in northern hemisphere winter due to increasing CO_2. *Climate Dyn.,* **12,** 467–476.

Edmon, H. J., B. J. Hoskins, and M. E. McIntyre, 1980: Eliassen–Palm cross sections for the troposphere. *J. Atmos. Sci.,* **37,** 2600–2616.

Hack, J. J., J. T. Kiehl, and J. W. Hurrell, 1998: The hydrologic and thermodynamic characteristics of the NCAR CCM3. *J. Climate,* **11,** 1179–1206.

Hall, N. M. J., B. J. Hoskins, P. J. Valdes, and C. A. Senior, 1994: Storm tracks in a high-resolution GCM with doubled carbon dioxide Quart. *J. Roy. Meteor. Soc.,* **120,** 1209–1230.

Held, I. M., and P. J. Phillips, 1993: Sensitivity of the eddy momentum flux to meridional resolution in atmospheric GCMs. *J. Climate,* **6,** 499–507.

Hoskins, B. J., I. N. James, and G. H. White, 1983: The shape, propagation and mean flow interactions of large scale weather systems. *J. Atmos. Sci.,* **40,** 1595–1612.

Hurrell, J. W., J. J. Hack, B. A. Boville, D. L. Williamson, and J. T. Kiehl, 1998: The dynamical simulation of the NCAR Community Climate Model Version 3 (CCM3). *J. Climate,* **11,** 1207–1236.

Kageyama, M., P. J. Valdes, G. Ramstein, C. Hewitt, and U. Wyputta, 1999: Northern Hemisphere storm tracks in present day and last glacial maximum climate simulations: A comparison of the European PMIP models. *J. Climate,* **12,** 742–760.

Kalnay, E., and Coauthors, 1996: The NCAR/NCEP 40-Year Reanalysis Project. *Bull. Amer. Meteor. Soc.,* **77,** 437–471.

Kiehl, J. T., J. J. Hack, G. B. Bonan, B. A. Boville, D. L. Williamson, and P. J. Rasch, 1998: The National Center for Atmospheric Research Community Climate Model: CCM3. *J. Climate,* **11,** 1131–1149.

Magnusdottir, G., and R. Saravanan, 1999: The response of atmospheric heat transport to zonally averaged SST trends. *Tellus,* **51A,** 815–832.

Pavan, V., 1996: Sensitivity of a multi-layer quasi-geostrophic β-channel to the vertical structure of the equilibrium meridional temperature gradient. *Quart. J. Roy. Meteor. Soc.,* **122,** 55–72.

——, N. Hall, P. Valdes, and M. Blackburn, 1999: The importance of moisture distribution for the growth and energetics of midlatitude systems. *Ann. Geophys.,* **17,** 242–256.

Peixoto, J. P., and A. H. Oort, 1992: *Physics of Climate*. American Institute of Physics, 550 pp.

Rayner, N. A., C. K. Folland, D. E. Parker, and E. B. Horton, 1995: A new global sea-ice and sea surface temperature (GISST) data set for 1903–1994 for forcing climate models. Hadley Centre Internal Note No. 69, 9 pp. [Available from the Hadley Centre, Met Office, London Road, Bracknell, Berkshire RG12 2SZ United Kingdom.]

Rind, D., 1998: Latitudinal temperature gradients and climate change. *J. Geophys. Res.,* **103,** 5943–5971.

Robinson, W. A., 2000: Review of the workshop on extratropical SST anomalies. *Bull. Amer. Meteor. Soc.,* **81,** 567–577.

Schubert, M., J. Perlwitz, R. Blender, K. Fraedrich, and F. Lunkeit, 1998: North Atlantic cyclones in CO2-induced warm climate simulations: Frequency, intensity, and tracks. *Climate Dyn.,* **14,** 827–837.

Stephenson, D. B., and I. M. Held, 1993: GCM response of northern winter stationary waves and storm tracks to increasing amounts of carbon dioxide. *J. Climate,* **6,** 1859–1870.

Thuburn, J., and G. C. Craig, 1997: GCM tests of theories for the height of the tropopause. *J. Atmos. Sci.,* **54,** 869–882.

Timbal, B., J.-F. Mahfouf, J.-F. Royer, and D. Cariolle, 1995: Sensitivity to prescribed changes in sea surface temperature and sea ice in doubled carbon dioxide experiments. *Climate Dyn.,* **12,** 1–20.

Trenberth, K. E., 1991: Storm tracks in the Southern Hemisphere. *J. Atmos. Sci.,* **48,** 2159–2178.

Ulbrich, U., and M. Cristoph, 1999: A shift of the NAO and increasing storm activity over Europe due to anthropogenic greenhouse gas forcing. *Climate Dyn.,* **15,** 551–559.